cy. 5

6P-4

MSFC
MTP-AERO-62-56
July 6, 1962

5dp

X64 12224

Code 2D

(NASA TMX 54508)

GEORGE C. MARSHALL SPACE FLIGHT CENTER

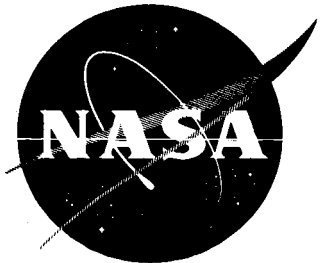## HUNTSVILLE, ALABAMA

AERODYNAMIC EVALUATION OF SA-2 FLIGHT (U)

By

F. S. GARCIA   *6 Jul. 1962*

NASA

(NASA-TM-X-54508)   AERODYNAMIC EVALUATION
OF SA-2 FLIGHT (NASA)   52 p

N74-71609

Unclas
00/99   29654

GEORGE C. MARSHALL SPACE FLIGHT CENTER

MTP-AERO-62-56

AERODYNAMIC EVALUATION OF SA-2 FLIGHT (U)

By F. S. Garcia

(U)   ABSTRACT   */2224*

A telemetered base pressure and surface pressure analysis was performed on the Saturn SA-2 vehicle, and comparisons were made to previous SA-1 results and/or wind tunnel test data. Telemetered accelerations, angles of attack, and engine deflections were also used to obtain the static stability ratio, gradient of normal force coefficient, and the center of pressure location of the vehicle. The axial force coefficient was obtained by the Flight Simulation Section, Flight Evaluation Branch, through an iterative process using observed atmospheric properties and adjusting the telemetered thrust and mass flow rates to coincide with the known trajectory.

The vehicle experienced a relatively uniform pressure distribution across the heat shield with the base drag being generally less than predicted by wind tunnel tests at the Rocket Test Facility, AEDC. The axial force coefficient coincided with SA-1 results and was less than predicted in the transonic and supersonic regions. Surface pressure readings showed close agreement with data from wind tunnel tests conducted at Langley Research Center.

The gradient of normal force coefficient was higher than predicted around the sonic region with values becoming less than predicted at supersonic Mach numbers. The flight determined center of pressure location oscillates with small deviations around the predicted curve in the transonic region, but becomes less than predicted in the supersonic regime.

Unel.   *AUTHOR*

GEORGE C. MARSHALL SPACE FLIGHT CENTER

MTP-AERO-62-56

July 6, 1962

AERODYNAMIC EVALUATION OF SA-2 FLIGHT (U)

By

F. S. Garcia

FLIGHT EVALUATION BRANCH
AEROBALLISTICS DIVISION

TABLE OF CONTENTS

(U) LIST OF ILLUSTRATIONS

(U)   LIST OF ILLUSTRATIONS (CONT.)

(U) DEFINITION OF SYMBOLS AND SUBCRIPTS

Symbol	Definition
a_L	Longitudinal acceleration
B^o	Angular acceleration due to outboard engine deflection
C_1	Angular acceleration due to unit angle of attack
C_{D_b}	Base drag coefficient
C_{m_α}	Gradient of moment coefficient about center of gravity per unit angle of attack
C_p	Pressure coefficient, $\dfrac{P - Pa}{q}$
C_x	Axial force coefficient
$C_z{}'$	Gradient of normal force coefficient per unit angle of attack
CG	Distance of center of gravity from gimbal plane
CP	Distance of center of pressure from gimbal plane
D	Reference diameter (6.528 m)
$\mathscr{D}_t$	Aerodynamic and internal fuel flow damping constant
F	Total axial thrust
F'	Engine thrust corrected for cant angle
I	Moment of Inertia
M	Mach Number
m	Total vehicle mass
P	Static pressure
q	Dynamic pressure
S	Reference area (33.98 m^2)

(U) DEFINITION OF SYMBOLS AND SUBCRIPTS (CONT.)

Symbol	Definition
S_B	Total base area
S_{B_N}	Total nozzle exit area
α	Free-stream angle of attack
β	Outboard engine angle deflection
γ	Ratio of specific heats for air (1.4)
$\ddot{\gamma}$	Normal acceleration
$\dot{\phi}$	Angular velocity
$\ddot{\phi}$	Angular acceleration

Subscripts	Definition
1,2 . . .	Indicate engine number
a	Ambient conditions
b	Base
L	Local surface conditions
o	Outboard engine
p	Pitch plane
y	Yaw plane

GEORGE C. MARSHALL SPACE FLIGHT CENTER

MTP-AERO-62-56

AERODYNAMIC EVALUATION OF SA-2 FLIGHT

By F. S. Garcia

(U) SUMMARY

A data analysis was performed on all telemetered pressures and
dynamic quantities influential to the aerodynamic behavior of the SA-2
vehicle. Aerodynamic parameters, calculated in their customary dimen-
sionless form, were mathematically smoothed; and comparisons were made
with SA-1 flight data, wind tunnel data and theoretical predictions.
An error analysis was performed on all telemetered data. Smoothed SA-1
data are shown as circled points in all graphs while the probable error
band is indicated by a dashed line.

Telemetered base pressure readings were analyzed for comparison
with wind tunnel test results and for the ultimate purpose of determining
the total base drag of the vehicle. The base drag of the vehicle deduced
from the telemetered measurements was less than predicted by wind tunnel
tests conducted at the Rocket Test Facility, AEDC.

Surface pressure measurements on the booster section, made for the
first time on SA-2, are in general agreement with results from wind
tunnel tests conducted at Langley Research Center. All surface pressure
measurements are plotted individually in this report in pressure coeffi-
cient form.

The axial force coefficient, obtained as a by-product of engine
performance evaluation, was generally less than predicted and practically
identical to SA-1 results. Values of C_{Z_α}, or C_Z', were higher than pre-
dicted around the sonic region with peak values occurring at Mach 1.15;
however, in the Mach number range between 1.5 and 3.6, C_Z' was somewhat
less than predicted. The center of pressure location was in general
agreement with predicted values up to M=2.0; after which SA-2 values
were consistently more aft than predicted.

(U) INTRODUCTION

To calculate and evaluate the over-all aerodynamic performance of a space vehicle, an accurate determination must be made of external pressure distributions, total and base drag, and of stability and control parameters. Base pressure measurements are of intrinsic value not only within themselves and to determine base drag, but also serve as a measure of the entire flow field and jet exhaust reactions around the base. Surface pressure measurements are significant especially when used to determine structural loads on items such as tanks, shields, etc. and to study the effects on small external protuberances commonly located on the surface of the vehicle.

The accurate knowledge of axial force is essential in any post-flight trajectory and performance analysis. Aerodynamic stability parameters are also important in predicting the control and structural strength requirements of a vehicle, and as a consequence, the winds through which a vehicle may safely pass. For this reason, it is important to verify theoretical and wind tunnel predictions of stability and moment characteristics with actual flight results of the type included herein.

This report presents an aerodynamic analysis on the SA-2 vehicle based mainly upon telemetered flight data. SA-1 data is also shown for comparison on the graphs together with values obtained either from the theory or from wind tunnel tests. Curves for SA-2 and SA-1 have been mathematically smoothed before inclusion in this report. In addition, an error analysis was performed on the data and probable 3σ error margins shown on all pertinent curves.

(U) DISCUSSION

A. Basic Aerodynamic Parameters and Trajectory Data

The SA-2 flight was identical to SA-1 when viewed in terms of basic free-stream aerodynamic parameters and trajectory data (Figures 1 to 6). Figure 1 shows the Mach number history; while Figures 2 and 3 show ambient pressure as a function of Mach number and time, respectively. Dynamic pressure and Reynolds number are plotted versus Mach number in Figures 4 and 5, respectively. Telemetered free-stream pitch and yaw angles of attack are plotted versus Mach number in Figure 6 and indicate close similarity with SA-1 results.

B. Analysis of Telemetered Pressure Data

1. Base Pressures

Base pressure instrumentation on SA-2 was identical to SA-1. The

ratios of base pressure to ambient pressure (P_b/P_a) as obtained from heat shield measurements D25-4, D25-7 and D38-4 are plotted versus Mach number in Figures 7 to 9. Base pressure data from these three measurements agree relatively well with each other; however, although readings from measurements D25-7 and D38-4 individually displayed the same trend as SA-1 results, measurement D25-4, located between the inboard and outboard engines, showed a deviation from SA-1 results. As shown in Figure 7, the two curves appear to be almost identical except for polarity. Since SA-2 data is in closer agreement with wind tunnel results in that it shows the expected uniform pressure distribution across the heat shield, it must therefore be concluded that measurement D25-4 on SA-1 was incorrect and was due to telemetry and/or measurement inaccuracies.

Base pressure readings at the center star flame shield, obtained through measurement D38-7, were in close agreement with SA-1 results. Because of the small area encompassed by the flame shield as compared to the entire effective base area, it was determined that the resultant force derived from this pressure would have little or no effect on the total base drag and was consequently neglected for this analysis. A more thorough pressure analysis on the center star region is presented in Reference 1.

The base pressure coefficients for the heat shield measurements were computed using the relation

$$CP_b = \frac{P_b - P_a}{q}.$$

(1)

and are plotted as a function of Mach number in Figures 10 to 12. Comparisons are also made to SA-1 results and wind tunnel test data. These figures indicate that in the transonic region an approximate minimum value of $CP_b = -0.11$ at M=1.15 was experienced by all three measurements.

Wind tunnel tests approximated the flight trajectory by simulating the Mach number and static pressure at altitude. The tests performed at the Rocket Test Facility, AEDC, were conducted on a 5.47 percent scale model of the SA-1 vehicle (Reference 2) and results presented in all graphs. Also shown are data from the 8x6 foot supersonic tunnel of the Lewis Research Center from tests conducted on a 3.70 percent scale model (References 2 and 3). AEDC data may be more reliable because as seen in Figures 2 and 4 the actual flight trajectory was more closely simulated.

4

The base pressure coefficient for all wind tunnel tests was obtained through the perfect gas form of Equation 1

$$C_{P_b} = \frac{P_b - P_a}{q} = \frac{P_b - P_a}{\frac{\gamma}{2} P_a M^2} = \frac{P_b/P_a - 1}{.7 M^2} \qquad (2)$$

2. Base Drag Coefficient

The base drag coefficient of the vehicle was calculated using a mean value of the computed individual base pressure coefficients on the heat shield.

$$C_{D_b} = -(C_{P_b})_{avg.} \frac{S_B - S_{B_N}}{S} \qquad (3)$$

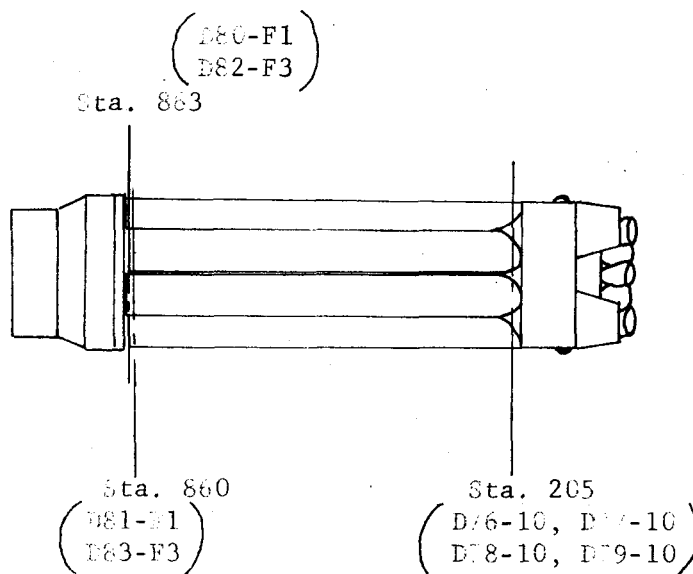where $S = \frac{\pi (6.528)^2}{4} = 33.98 m^2$ (reference area)

$\frac{S_B - S_{B_N}}{S} = 0.7$ (effective base area correction to account for all nozzle exit areas)

Measurements obtained from wind tunnel data and both Saturn flights (except data from measurement D25-4 on SA-1) seem to support the adequacy of using a straight average of C_{P_b} in computing the base drag coefficient since all readings closely exhibited the same trend. The base drag coefficient for SA-1 shown in Figure 13 still includes measurement D25-4, which was considerably different from the average of the other two measurements. If data from the SA-3 flight supports SA-2 results with respect to measurement D25-4, the SA-1 results will be revised accordingly. Calculated values of C_{D_b} are shown versus Mach number in Figure 13, and SA-1 results are shown for comparison. A predicted curve based on AEDC wind tunnel data is also shown on the graph. As shown in the figure, base drag was generally lower than predicted. A positive pressure thrust due to reverse flow of exhaust gases was attained at approximately M=1.7.

3. Surface Pressures

Eight pressure measurements were installed in the surface of the booster section at Stations 205, 860, and 863. This instrumentation was not installed on the SA-1 vehicle. The approximate longitudinal locations of the pressure orifices are shown on the sketch below. Pressure data obtained from these measurements were converted to pressure coefficient form and plotted versus Mach number. Results obtained from

wind tunnel tests conducted on a 1.6 percent scale model of the vehicle at the Langley 8 foot TPT and Langley 4 foot UPWT are shown on the graphs for comparison (References 4 and 5)

$$\left(\begin{array}{c} D80-F1 \\ D82-F3 \end{array}\right)$$

Sta. 883

$$\left(\begin{array}{c} D81-F1 \\ D83-F3 \end{array}\right)$$

Sta. 860

Sta. 205

$$\left(\begin{array}{c} D76-10, \ D77-10 \\ D78-10, \ D79-10 \end{array}\right)$$

Booster Section Showing Longitudinal
Location of Surface Pressure Measurements

a) Station 205   Four local static pressure gauges were located on the fillets of the flared-out region on an intermediate point adjacent to the extreme lower portion of the fuel and LOX tanks. Their respective radial location is shown individually on each graph (Figures 14 to 17). Each measuring gauge consists of a pressure actuated potentiometer providing a linear output with applied pressure. The unit is manufactured by Trans-Sonics, Inc., Burlington, Mass., and has a measuring range of 0 - 20 psia.

When converted to pressure coefficient form, data from measurements D76-10, D77-10, and D79-10 agree relatively well with each other showing positive values of Cp_L throughout (Figures 14 to 17). However, as shown in Figure 16, measurement D78-10 deviates from this trend by having a sharp drop in Cp_L which reaches negative values before M=2.0 and remain negative throughout. Considering wind tunnel data and readings obtained at similar locations by the other three measurements, the most likely explanation at this time for this deviation is telemetry and/or measurement error. Additional flight tests will be necessary to verify this

conclusion. In general, wind tunnel test data ($\alpha = 4^{\circ}$) at this station are in close agreement with flight results, although the pressure taps in the wind tunnel model were located in the tanks and not on the fillets. A comparison of this type may or may not be valid depending on the actual flow field at this location.

b) Stations 860 and 863 Pressure gauges for measurements D81-F1 and D83-F3 at Station 860 were located on the skin of fuel container units 1 and 3, respectively, facing the center of the cluster. Details on the location and installation of these measurements are shown in Figures 18 and 19. Measurements D80-F1 and D82-F3 at Station 863 were also located in fuel container units 1 and 3, respectively, but the orifices were in the end ring frame facing the flight direction (Figure 20). Each of the gauges discussed above consisted of a pressure transducer containing a pressure responsive capsule which actuates a precision potentiometer providing a linear output with applied pressure. The gauges were made by G.M. Giannini & Co., Inc., Pasadena, California, and have a measuring range of 0-20 psia.

Pressure data (C_{P_L}) from the foregoing measurements are plotted versus Mach number in Figures 21 to 24. All pressure readings maintained a negative value of C_{P_L} throughout and agree very closely with each other. Wind tunnel data at this location nearly coincided with flight results.

4. Error Analysis on Telemetered Pressures

An error analysis was performed on all parameters which were functions of telemetered pressure data. Possible deviations from calculated values are shown on each graph as a band around the SA-2 curve and indicated by a dashed line. A telemetered base pressure and surface pressure error margin equivalent to 2% of the measuring range of the gauges, i.e., $\pm$ 281 kp/m^2, was arbitrarily used for the entire flight on the basis of previous experience. Telemetered data was mathematically smoothed, and except for base pressure measurement D25-4 on the SA-1 vehicle, all SA-1 base pressure data fell within the error band determined by the SA-2 curves.

C. Axial Force and Stability Parameter Analysis

Axial force and aerodynamic static stability parameters were determined from SA-2 measured data and comparisons have been made to previous SA-1 flight and wind tunnel results. The small values of yaw angle of attack and subsequently low normal accelerations confined the stability analysis to the pitch plane only.

1. Axial Force Coefficient (C_X)

The axial force coefficient was determined by the Flight Simulation Section, Flight Evaluation Branch, (Reference 7) with a method whereby the "telemetered" thrust* and mass flow rates are adjusted to fit a simulated trajectory to the reference tracking trajectory. This is accomplished by assuming the "telemetered" thrust and mass flow rates to be known and computing a preliminary trajectory. Through partial derivatives from the actual postflight trajectory, new values of thrust and mass flow rate are obtained. With these new values of thrust and mass flow rate, C_X is determined by the relation

$$C_X = \frac{F - ma_L}{qS}$$ (4)

By alternately solving for thrust and mass flow rate, the procedure above is repeated until the simulated trajectory converges to the reference tracking trajectory which, in each case, gives a new value of C_X from Equation 4.

Figure 26 is the plot of axial force coefficient versus Mach number. Also shown in the figure are the data obtained from SA-1 flight and the values predicted in Reference 6. SA-2 values are, for all practical purposes, identical to SA-1. As shown in the figure, the axial force coefficient is roughly 15% less than predicted for Mach numbers above 0.7. In terms of over-all vehicle performance, this reduction in axial force is equivalent to a 0.25 sec longer burning time for SA-2 and SA-1.

Theoretical analyses have shown that the angle of attack influence on axial force may be neglected for total angles of attack under 15 degrees, which as shown in Figure 6, is the case for the two Saturn flights.

2. Axial Force Minus Base Drag

To estimate the accuracy of methods used to predict the wave, viscous and interference drag contributions to the total axial force, the base drag coefficient (Figure 13) was subtracted from the axial force coefficient

---

* Thrust obtained by means of telemetered engine chamber pressures

(Figure 26), and the result plotted versus Mach number in Figure 27. SA-1 and SA-2 results agree very well with each other above M=1.5, being on the average about 9% lower than predicted.

3. Gradient of Normal Force Coefficient (C_z')

The gradient of the normal force coefficient ($C_{z\alpha}$ or C_z') was obtained using telemetered values of angle of attack, normal acceleration, and engine deflection;

$$C_z' = \frac{m\ddot{y} - \Sigma F'_o\beta}{qS\alpha} \qquad (5)$$

where

$$\Sigma F'_o\beta = F'_1\beta_1 + F'_2\beta_2 + F'_3\beta_3 + F'_4\beta_4 = \text{total normal thrust component.}$$

C_z' is plotted as a function of Mach number in Figure 28. SA-1 flight data is also shown in the figure together with predicted values based upon wind tunnel tests (Reference 6). As shown in this graph, SA-2 values around the sonic region were higher than predicted; C_z' reached a maximum value of approximately 3.3 at M=1.15 compared to a predicted value of 3.1 at M=1.0. Flight values were less than predicted for the Mach number range between 1.5 and 3.6. The SA-1 curve, shown for comparison on the graph, is also characterized by having higher values of C_z' around the sonic region (a peak value of approximately 3.7 occurring at M=1.10). The dubious magnitude of this peak can be verified one way or the other only through additional flight tests.

4. Center of Pressure Location (CP/D)

The center of pressure of the vehicle was computed through the relationship

$$\frac{CP}{D} = \frac{CG}{D} + \frac{1}{C_z'\alpha qSD} \left[\Sigma F'_o\beta(CG) + I\ddot{\varphi} + \mathscr{D}_t\dot{\varphi}\right] \qquad (6)$$

using the smoothed values of C_z' from Figure 28 where

- $\frac{CP}{D}$ = center of pressure location from Sta. 100 (calibers)

$\frac{CG}{D}$ = center of gravity location from Sta. 100 (calibers)

$\mathscr{D}_t$ = aerodynamic and internal fuel flow damping constant (kp-m-sec).

Values of CP/D obtained by use of Equation 6 are shown plotted versus Mach number in Figure 29 together with a predicted curve (Reference 6) based on wind tunnel results. SA-1 data are also shown on the graph. As shown in the figure, SA-2 results are in general agreement with the predicted curve up to M=2.0, after which values of CP/D were generally slightly more aft than predicted. SA-2 flight data did not show a sharp minimum point as experienced from predicted values at M=1.0. SA-1 data were in close agreement with SA-2 results except that values of CP/D after M=2.0 fell more forward (closer to predicted) than SA-2.

5. Gradient of Moment Coefficient About C.G. (C_{m_α})

The gradient of the moment coefficient was obtained from the relationship

$$C_{m_\alpha} = \left(\frac{CP}{D} - \frac{CG}{D}\right) C_z' \tag{7}$$

where the values of C_z' and CP/D are those in Figures 28 and 29, respectively. Values of C_{m_α} are shown as a function of Mach number in Figure 30 together with SA-1 results and a predicted curve. SA-2 calculations show values of C_{m_α} generally less (more stable) than predicted in the supersonic regime. As shown in Figure 30, SA-1 experienced values of C_{m_α} higher (more unstable) than predicted or SA-2 around Mach 1. This occurrence was mostly due to the questionably higher peak in C_z' for SA-1 (Figure 28), which in turn was used to compute C_{m_α} from Equation 7.

6. Ratio of Gradients of Angular Acceleration (C_1/B^o)

The ratio of gradients of angular acceleration (static stability ratio) of the vehicle was determined through the relation

$$\frac{C_1}{B^o} = \frac{C_z' qSD\left(\frac{CP}{D} - \frac{CG}{D}\right)}{\Sigma F_o' CG} = \frac{-C_{m_\alpha}qS}{\Sigma F_o' \frac{CG}{D}} \tag{8}$$

where

$$\Sigma F_o' = F'_1 + F'_2 + F'_3 + F'_4 = \text{total thrust of outboard engines corrected for cant angle.}$$

C_1/B^o is plotted versus Mach number in Figure 31 and compared to a predicted curve based on the SA-2 trajectory. SA-1 results are also shown on the figure. C_1/B^o is considerably more positive than predicted (in the order of 10%) in the supersonic regime. The curve of C_1/B^o for SA-1, as in the C_{m_α} curve, indicates greater vehicle instability around

the sonic region, stemming mainly from the considerably higher values of C_z' for that vehicle.

7. **Drag and Stability Parameter Error Analysis**

A probable error band was determined for SA-2 aerodynamic curves, based upon individual arbitrary error values assigned to telemetered readings of angle of attack, normal acceleration, angular velocity, and engine deflections. The error margins for C_z', CP/D, and C_{m_α} are computed taking the root mean square value of the total error determined through the use of partial derivatives.

Because of the uncertainty in the errors associated with the iteration procedure used for the engine performance evaluation, it was felt that it may be difficult to estimate accurately the absolute error in the axial force coefficient (C_X) which is a by-product of the engine evaluation. For this reason, the percentage variation in the axial force coefficient observed from Jupiter ballistic missile flights (Reference 8) has been used to determine the probable error bands in C_X. However, the close agreement between the SA-1 and SA-2 curves indicates that the reliability may be greater than indicated by these error margins. An error analysis performed by Flight Simulation Section, Flight Evaluation Branch, also supports this. The improvement over the results obtained for the Jupiter is due to improvements in the engine performance evaluation programs.

Error bands around SA-2 data are shown as dashed lines on all curves. Data from both flights and the predicted values fell within these bands.

(U) CONCLUSIONS

Analysis of telemetered data for the SA-2 vehicle indicate the following conclusions:

1. The base drag coefficient was lower (50% at M=1) than predicted up to approximately M=3.

2. The axial force coefficient for SA-2 coincided with SA-1 results and was on the average about 15% lower than predicted for supersonic Mach numbers up to M=3.

3. Surface pressure measurements at Stations 205, 860 and 863 agreed relatively well with test data obtained at the Langley Research Center 8 foot TPT and 4 foot UPWT.

4. The gradient of normal force coefficient, C_z', reached a maximum value of approximately 3.3 at M=1.15 compared to a predicted value of 3.1 at

M=1.0. In the Mach number range between 1.5 and 3.6, $C_Z{'}$ was lower than predicted.

5. The center of pressure location, CP/D, was in general agreement with predicted values up to M=2.0, after which the location was consistently more aft than predicted. A sharp rearward shift during the transonic regime was experienced in wind tunnel tests (predicted) but not on SA-2 or SA-1.

6. The gradient of moment coefficient about the center of gravity, C_{m_α}, was generally more negative than predicted (more stable) in the supersonic regime.

(U) REFERENCES

1. Saturn Flight Evaluation Working Group, MSFC, Saturn SA-2 Flight Evaluation, MPR-SAT-WF-62-5, June, 1962 (C)

2. Jones, I.P., Some Additional Results and Analysis of the AEDC Saturn SA-1 Hot Jet Tests, M-AERO-AH Memorandum No. M-AERO-A-39-62, June 1962

3. Lewis Research Center, Preliminary Results Obtained from the 1/27 Scale Saturn Base Heating Tests in the Lewis 8x6 Foot Supersonic Tunnel, October 1961

4. Windham, J.O., Pressure Distribution Along a Model Saturn C-1 Block I Vehicle, MSFC Aeroballistics Division, Aero Internal Note 7-62, March 1962

5. Windham, J.O., Results of Wind Tunnel Investigations of the Tank Loads on a 1.6 Percent Model of the Saturn SA-1 Configuration, MSFC Aeroballistics Division, Internal Note 12-61, August 1961

6. MSFC Aeroballistics Division, Control-Stability Data Report for Saturn Vehicle SA-1, MTP-AERO-61-39, April 1961 (C)

7. Memorandum to Chief, Experimental Aerodynamics Branch, M-AERO-E, from Chief, Flight Evaluation Branch, M-AERO-F, Axial Force Coefficient, July 5, 1962

8. Weisler, A.C. and Hagood, C.C., Jupiter Summary Report, Volume VI, ABMA Report No. RJ-TR-61-10, June 1961

9. Garcia, F.S., Flight Evaluation of Axial Force and Base Pressure for Saturn SA-1, MTP-AERO-62-15, February, 1962

10. Saturn Flight Evaluation Working Group, MSFC, Saturn SA-1 Flight Evaluation, MPR-SAT-WF-61-8, December 1961 (C)
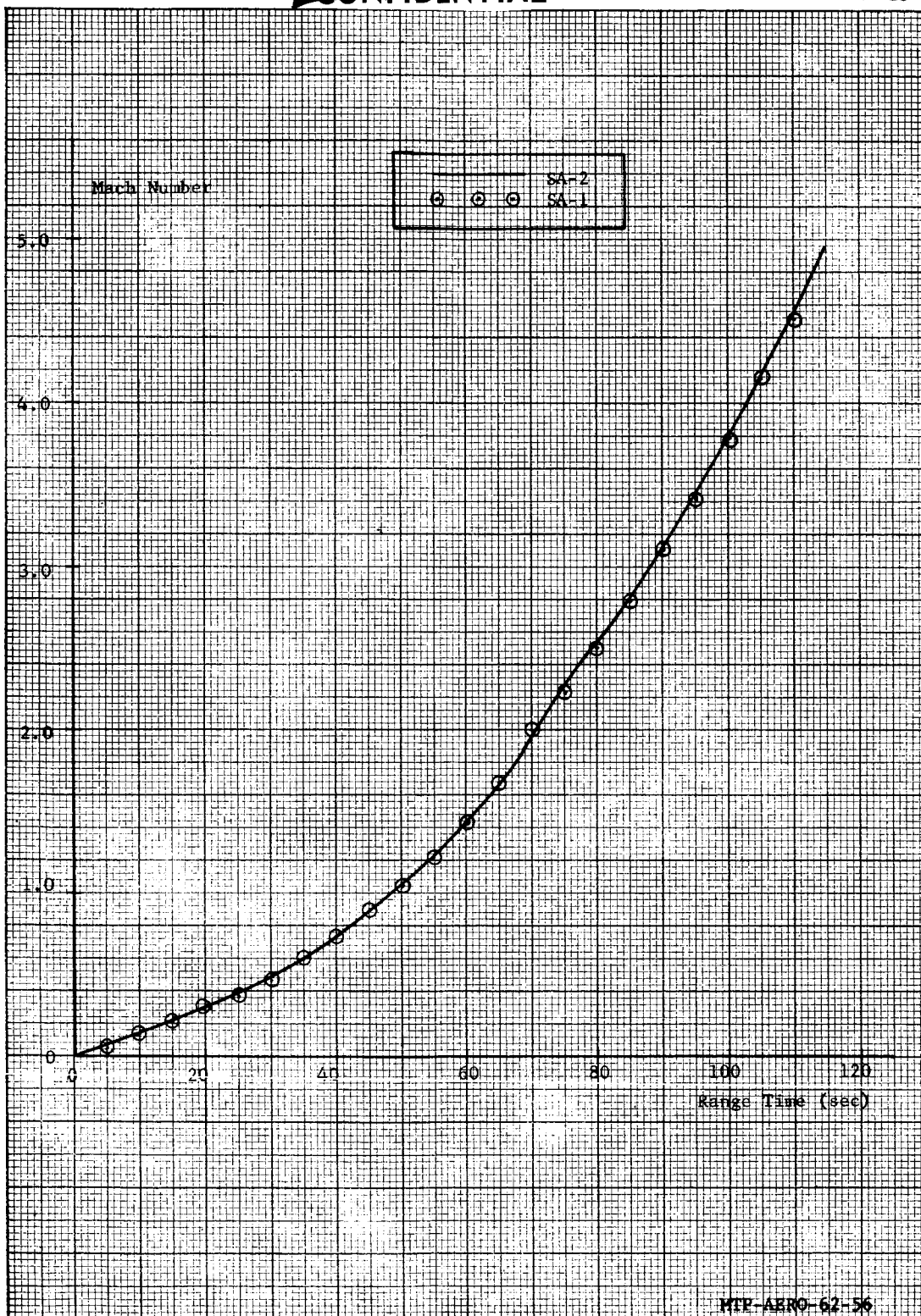
Fig. 1   Mach Number Versus Range Time
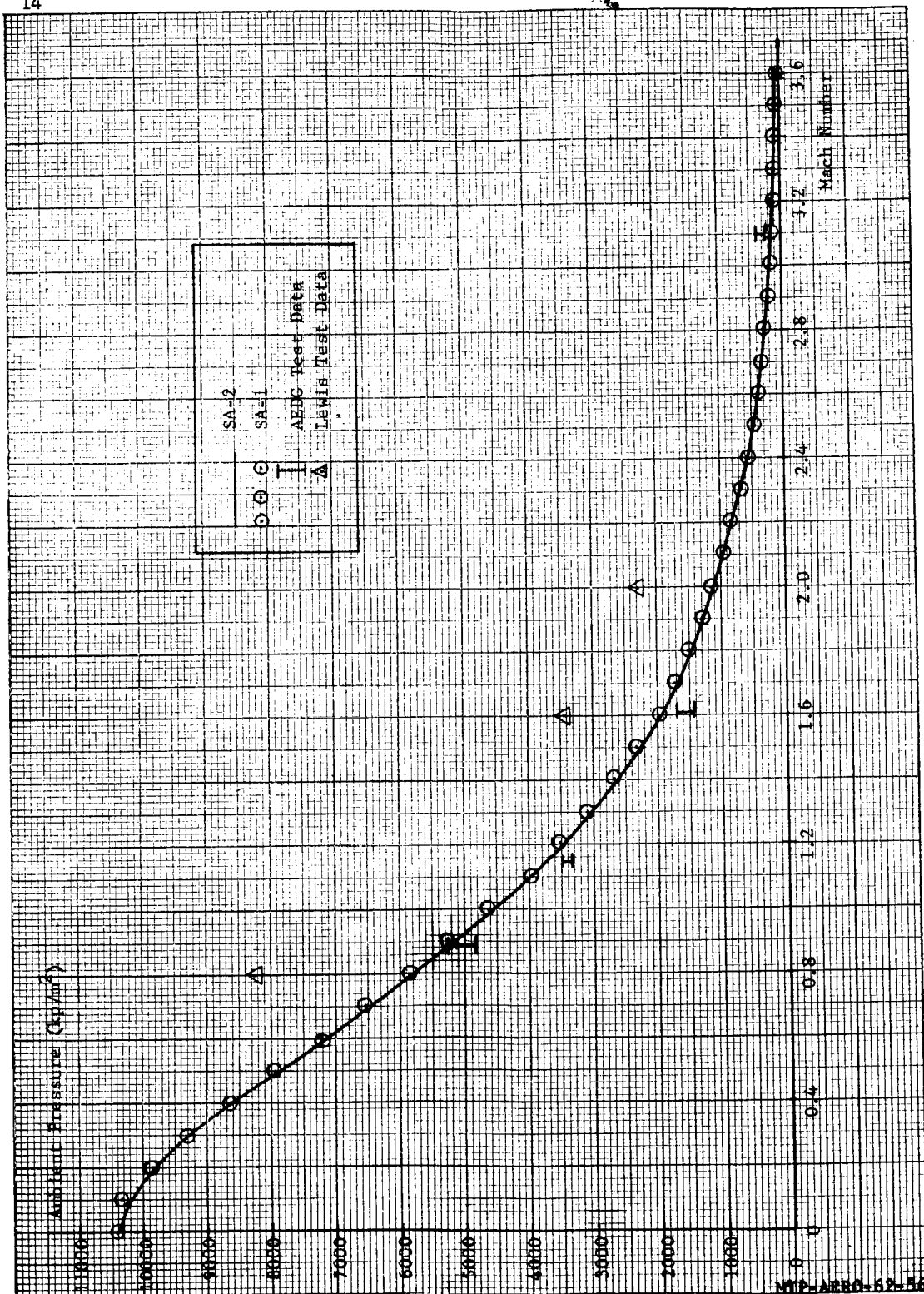
Fig. 2 Ambient Pressure Versus Mach Number
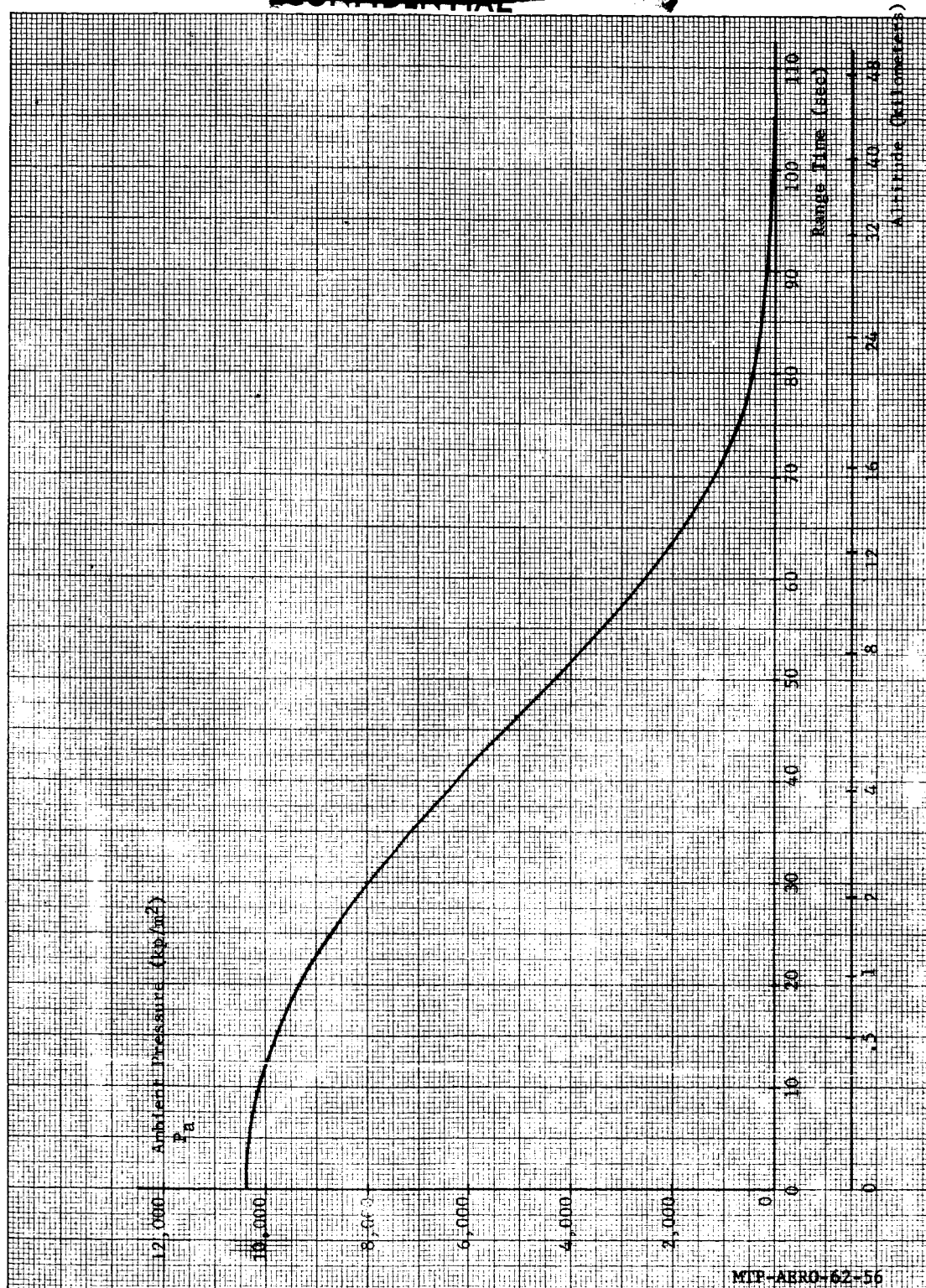
Fig. 3 Ambient Pressure Versus Range Time For SA-2

MTP-AERO-62-56

Dynamic Pressure (kp/m²)

Legend:
- SA-2
- SA-1
- AEDC Test Data
- Lewis Test Data*

* Note: Not included in the graph are dynamic pressure readings of 6089 kp/m² at M=1.6 and 6357 kp/m² at M=2.0 from Lewis wind tunnel tests.
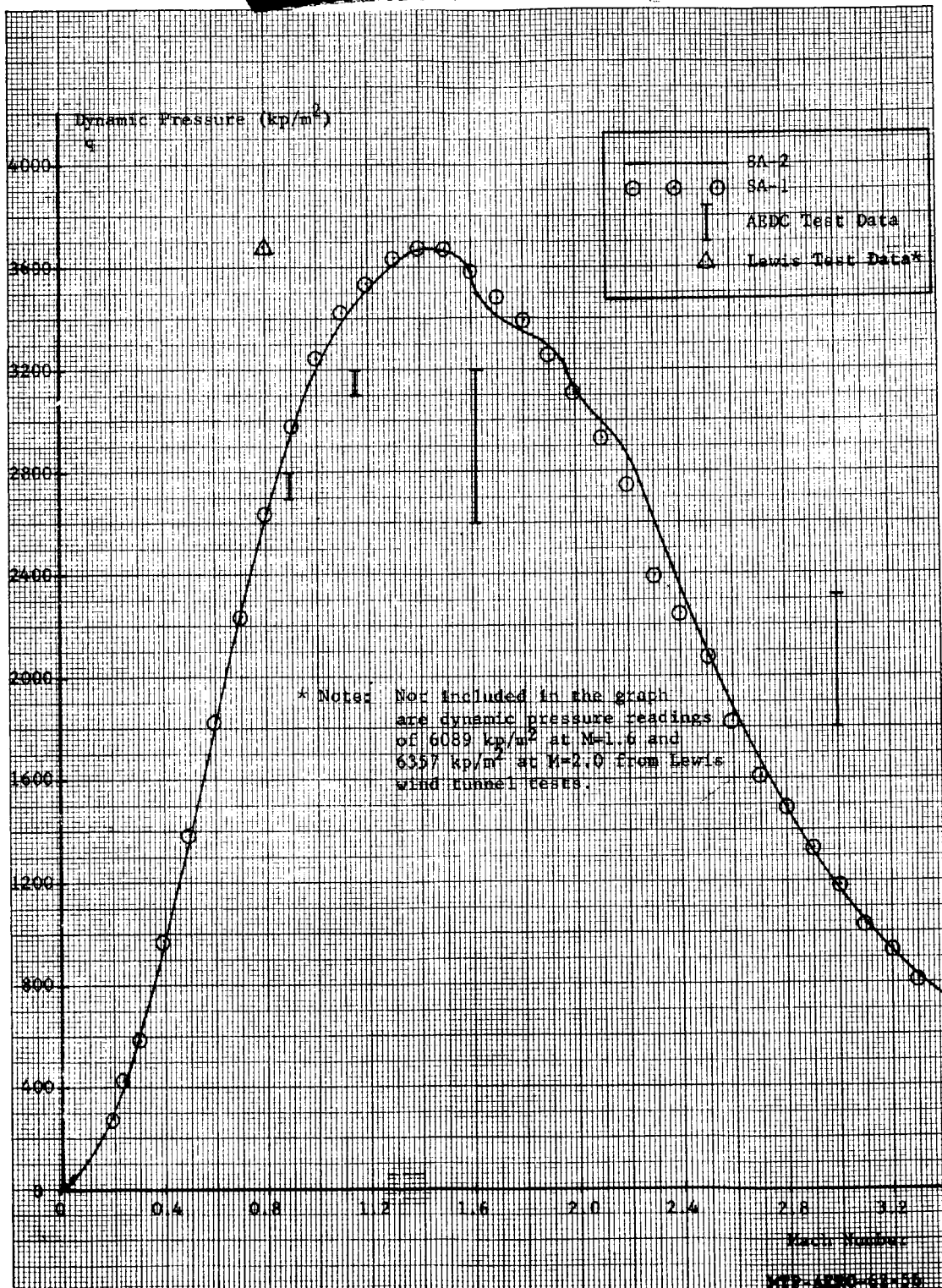
Mach Number

Fig. 4   Dynamic Pressure Versus Mach Number
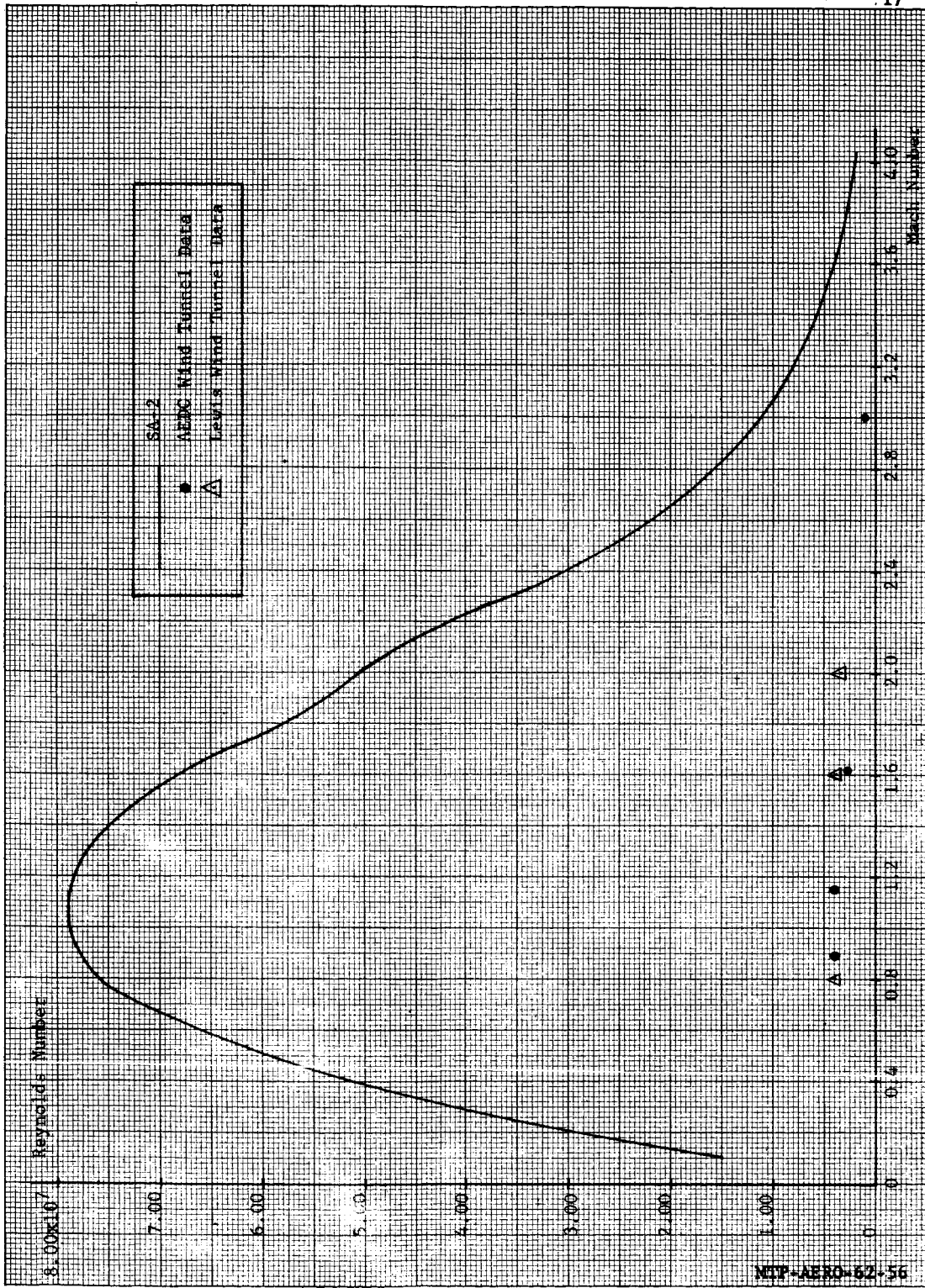
Fig. 5 Reynolds Number (Based on Reference Body Diameter) Versus Mach Number

18

Pitch Free-stream Angle of Attack (deg)

Mach Number

Yaw Free-stream Angle of Attack (deg)

Mach Number

SA-2 Telemetered Data
SA-1 Telemetered Data

MTP-AERO-62-36
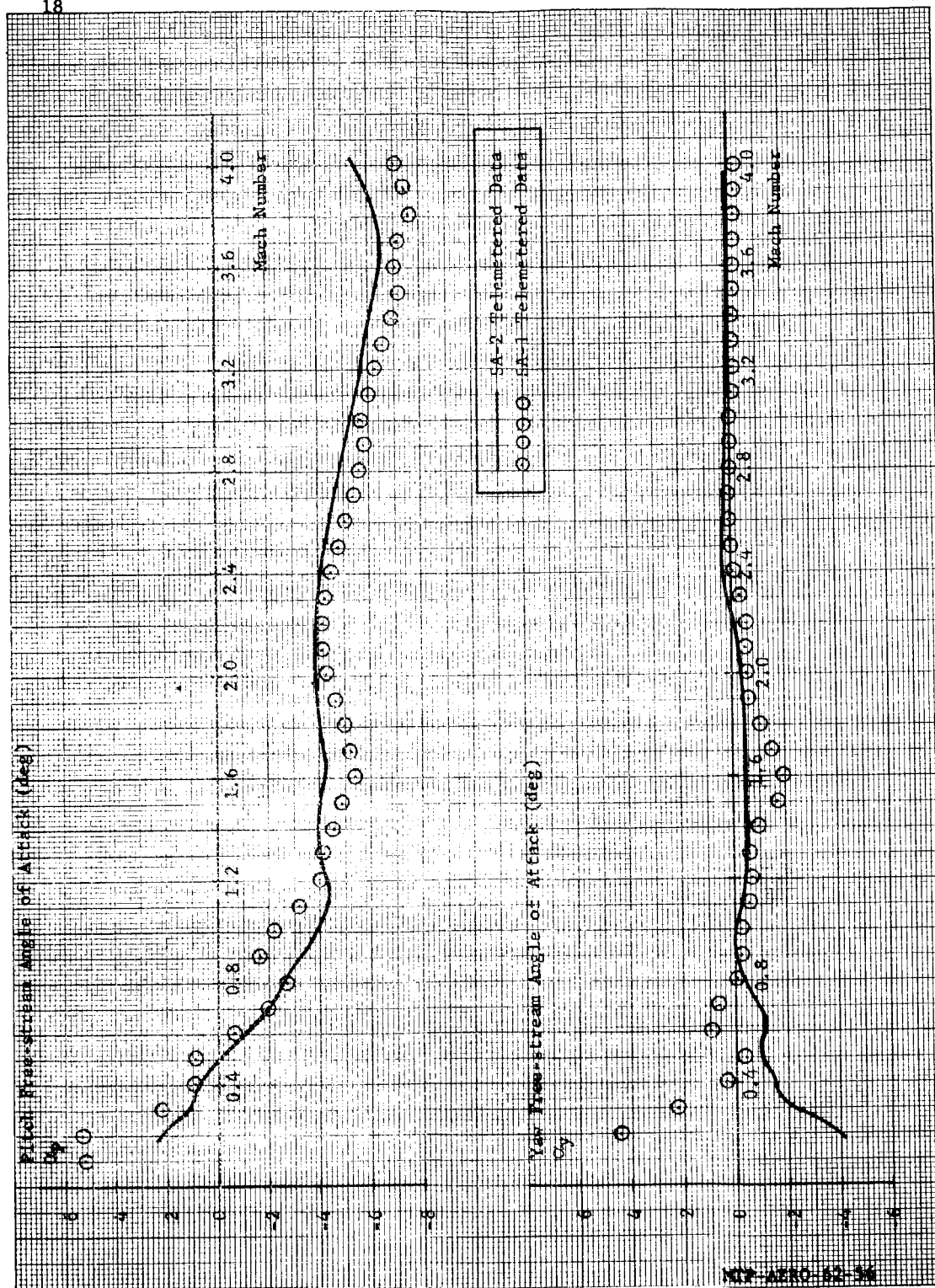
Fig. 6   Free Stream Angles of Attack Versus Mach Number
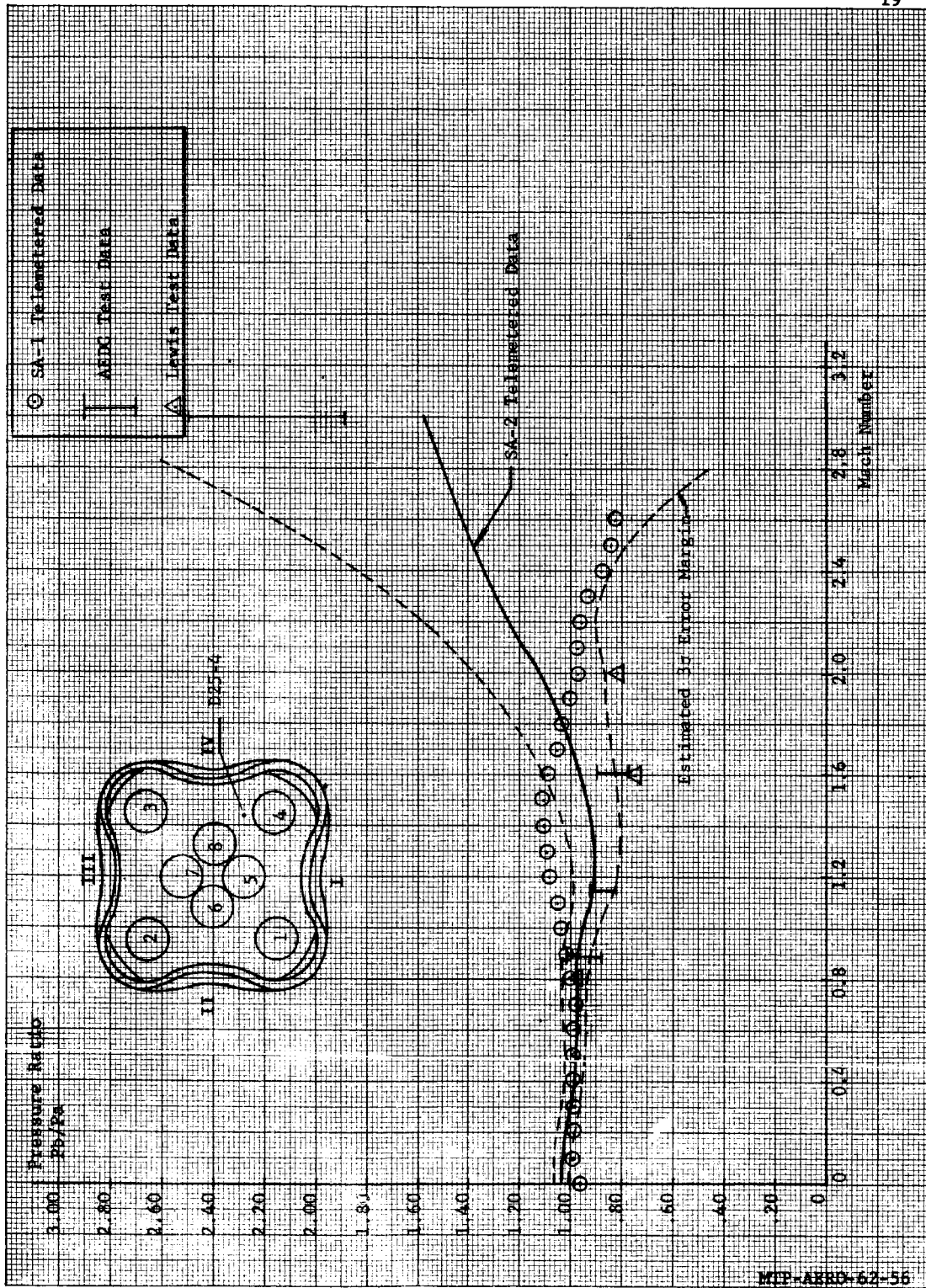
Fig. 7   Ratio of Base Pressure To Ambient Pressure Versus Mach Number For Measurement D25-4

MTP-AERO-62-56
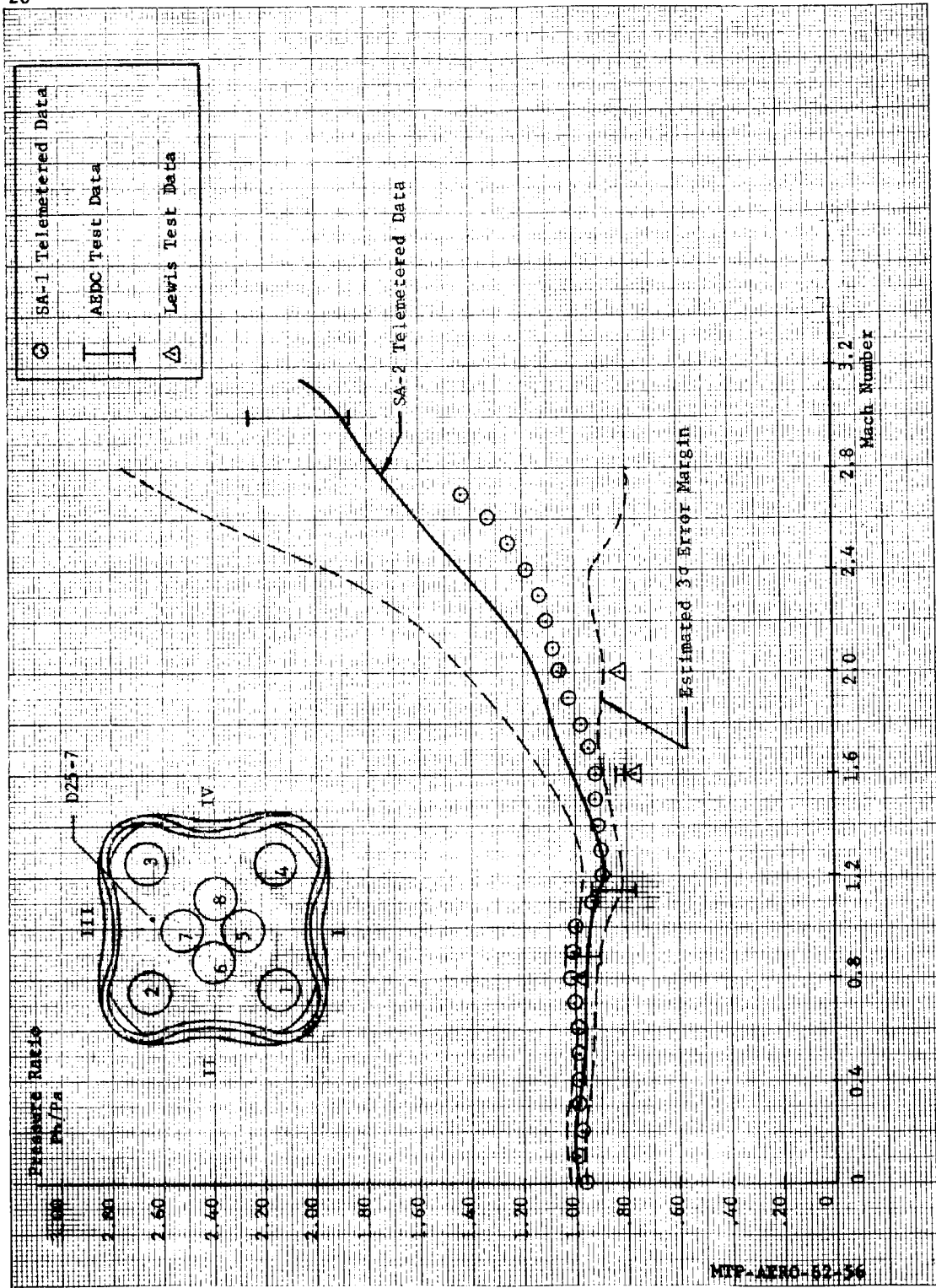
Fig. 8   Ratio of Base Pressure To Ambient Pressure Versus Mach Number For Measurement D25-7
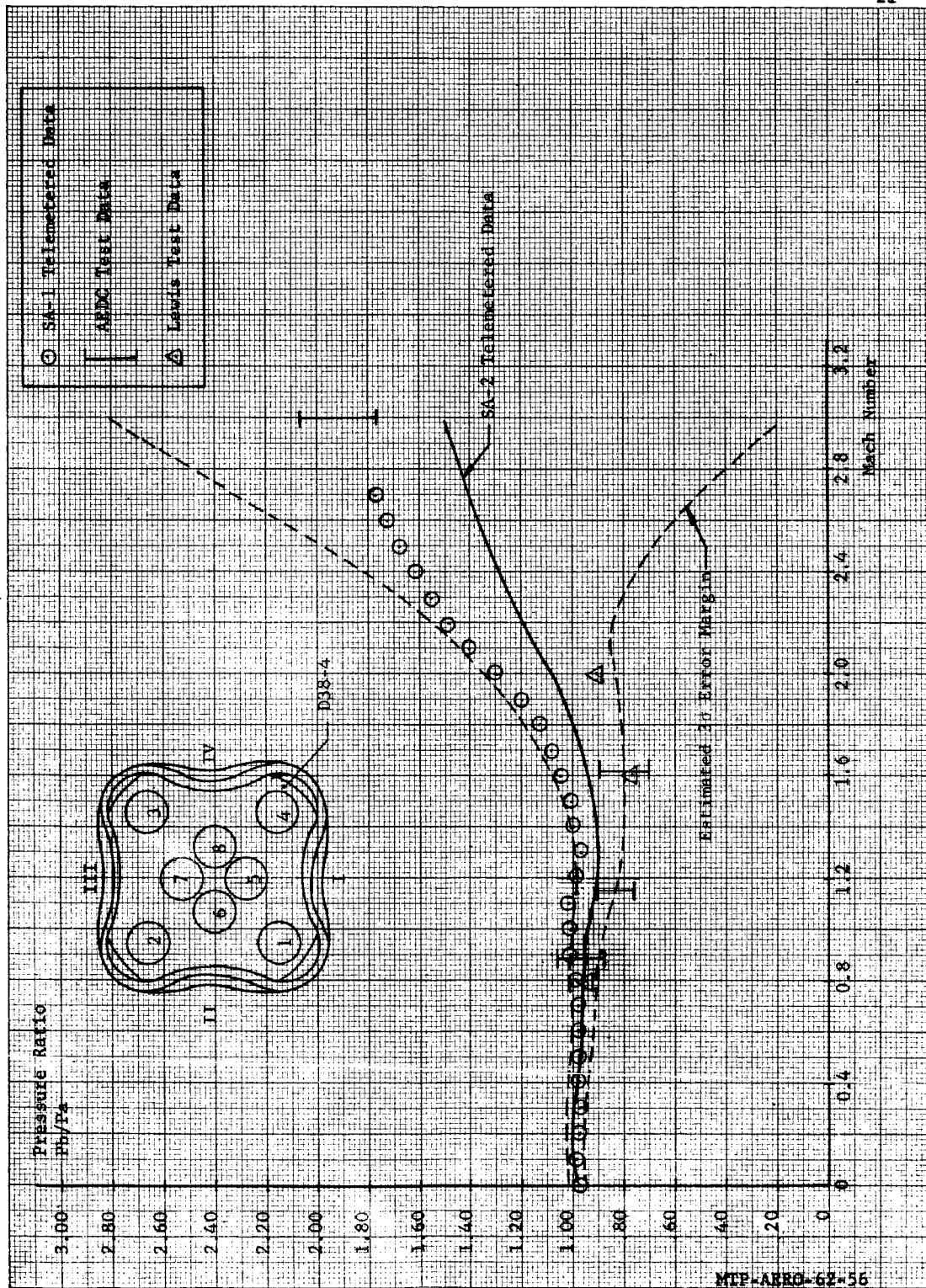
Fig. 9   Ratio of Base Pressure To Ambient Pressure Versus Mach Number For Measurement D38-4
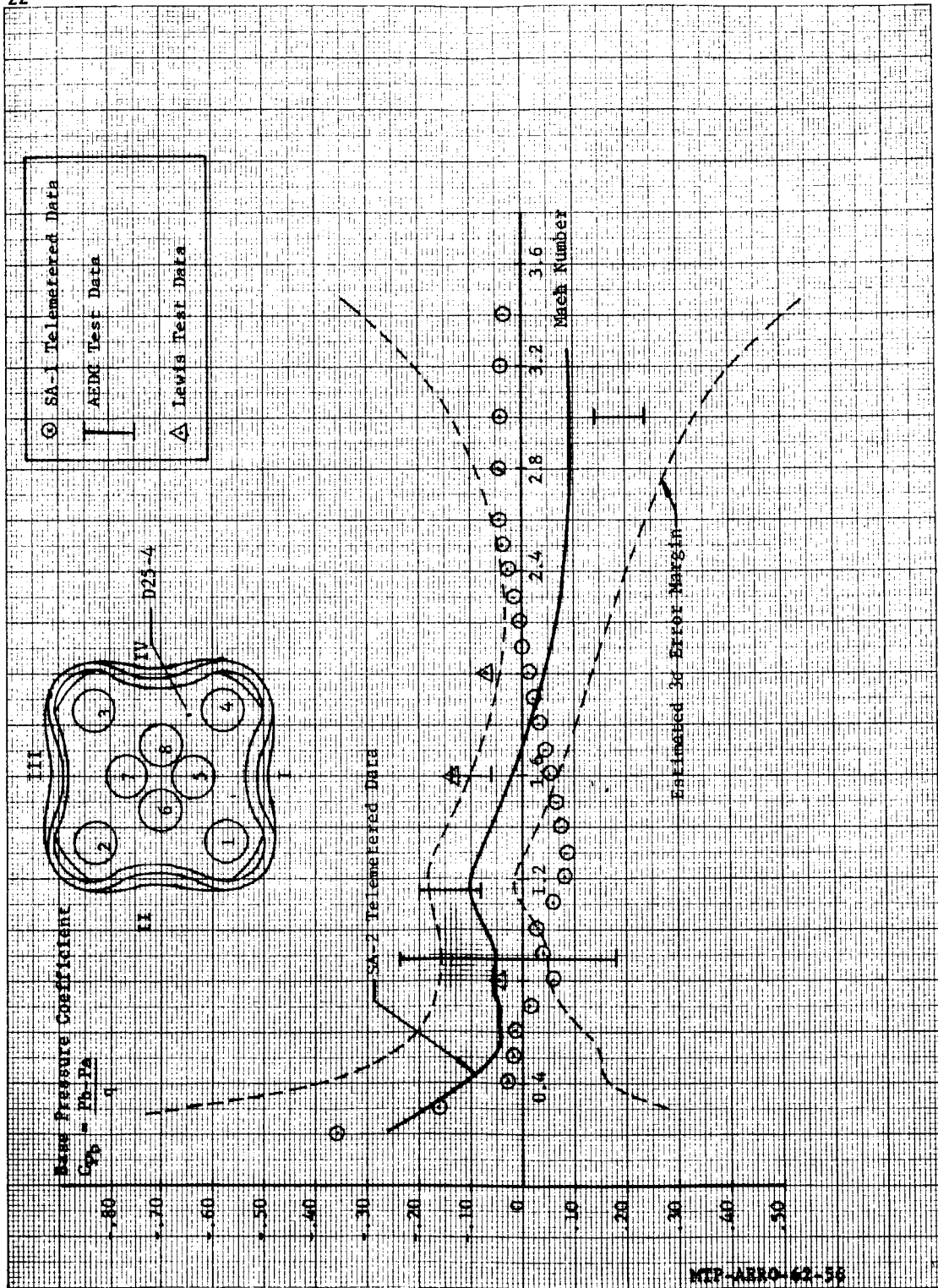
Fig. 10   Base Pressure Coefficient Versus Mach Number For Measurement D25-4

Fig. 11   Base Pressure Coefficient Versus Mach Number For Measurement D25-7
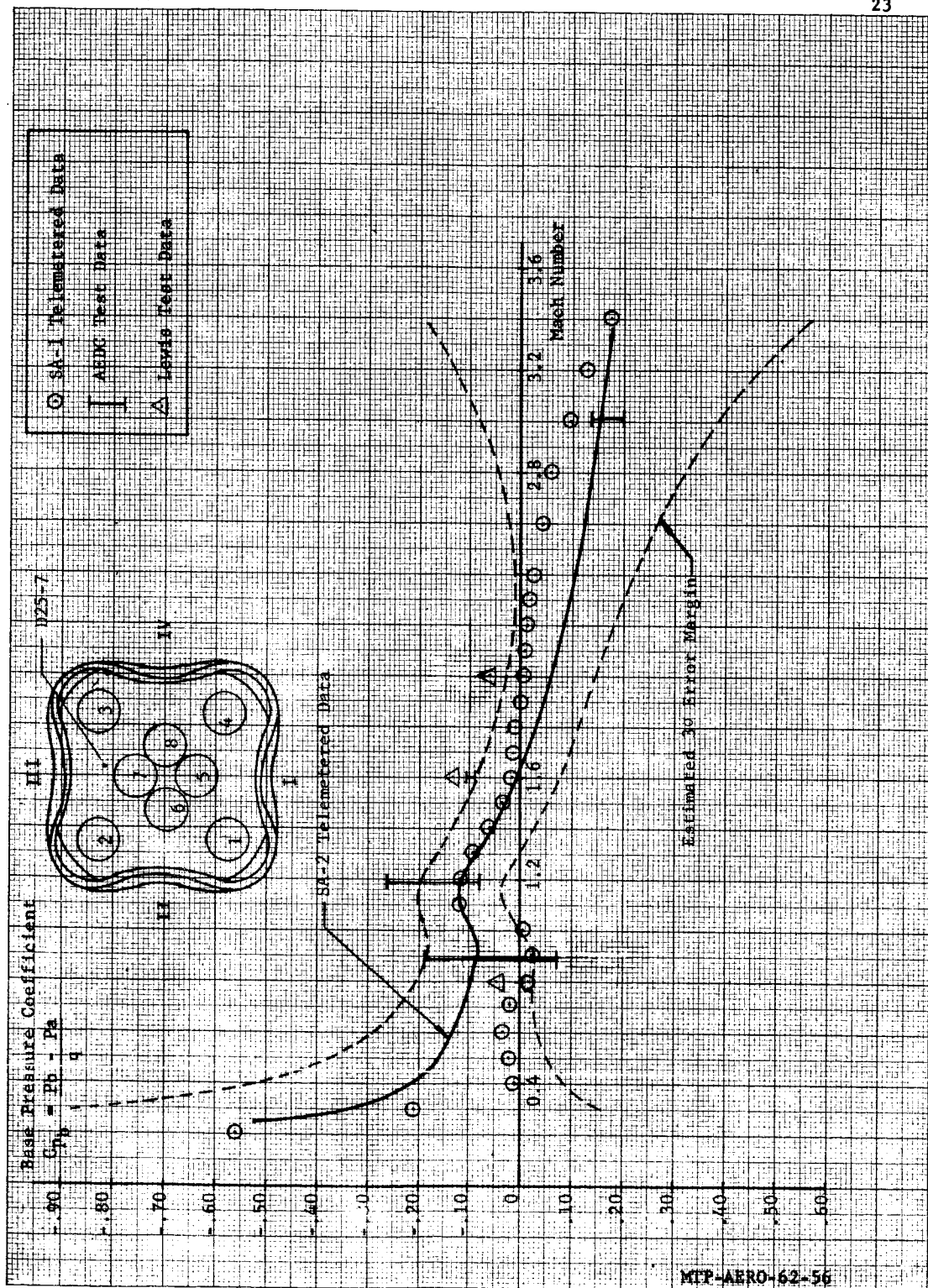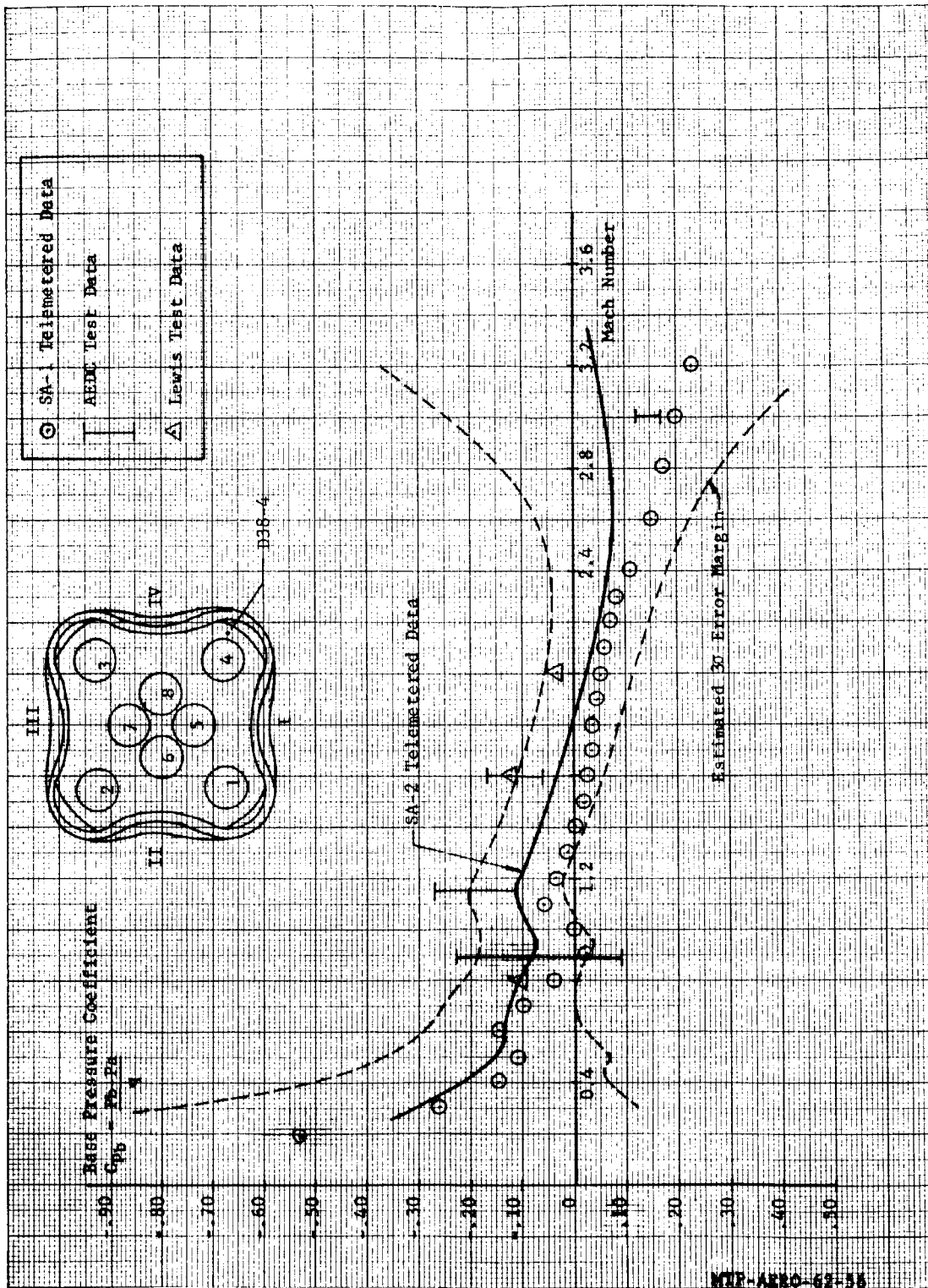
Fig. 12   Base Pressure Coefficient Versus Mach Number For Measurement D38-4
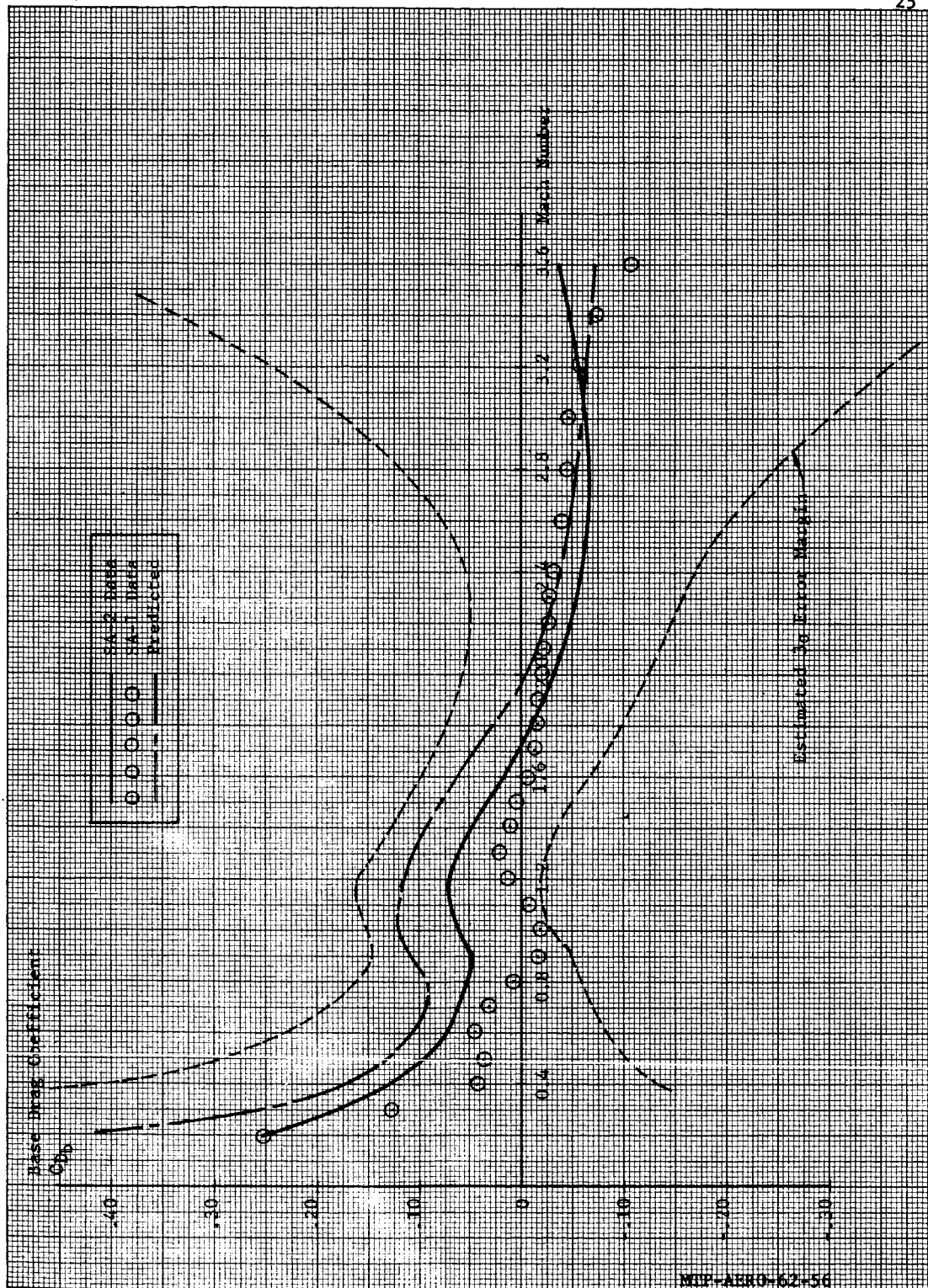
Fig. 13 Base Drag Coefficient Versus Mach Number

MTP-AERO-62-56
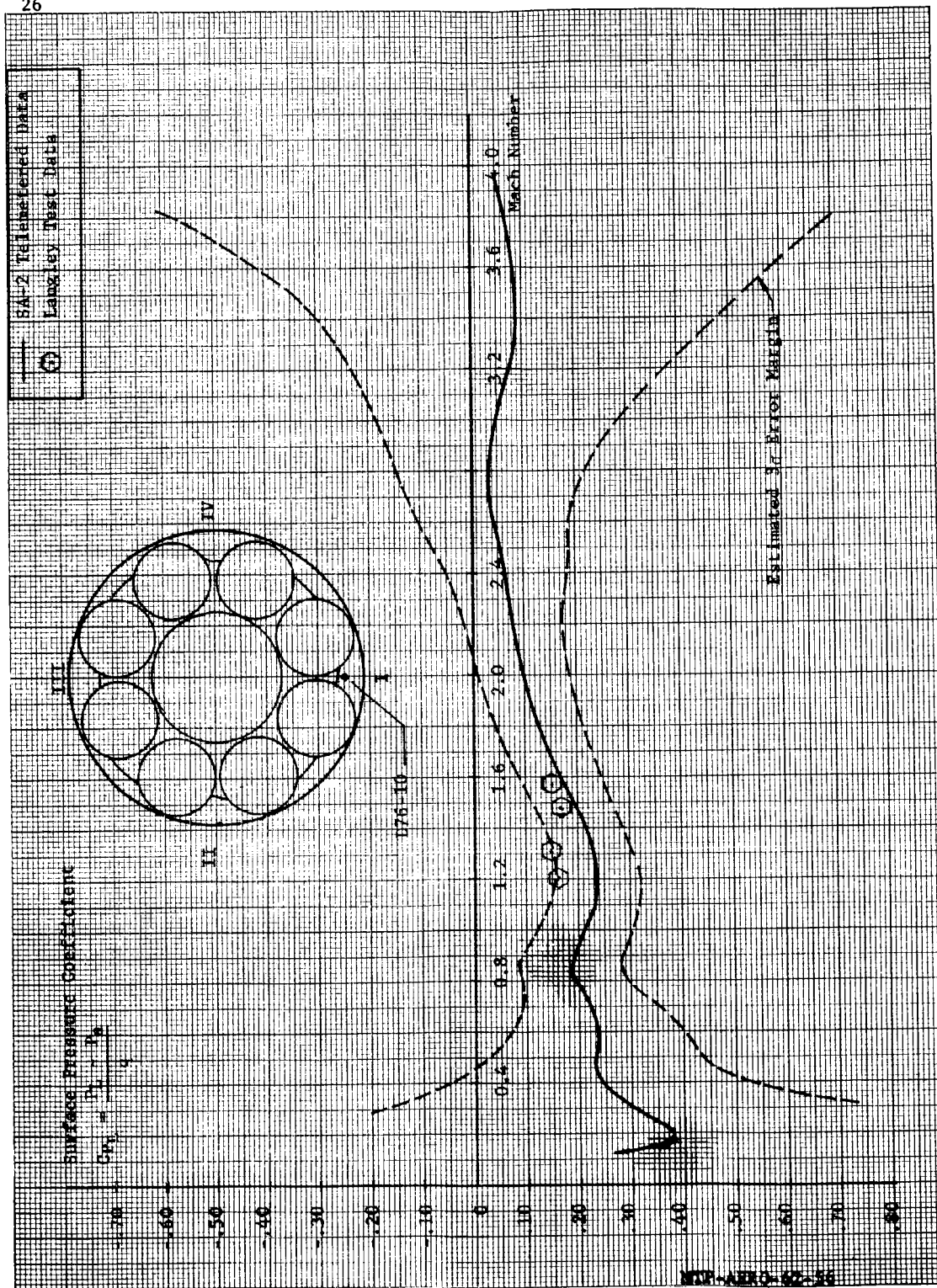
Fig. 14 Surface Pressure Coefficient Versus Mach Number for Measurement D76-10 at Station 205
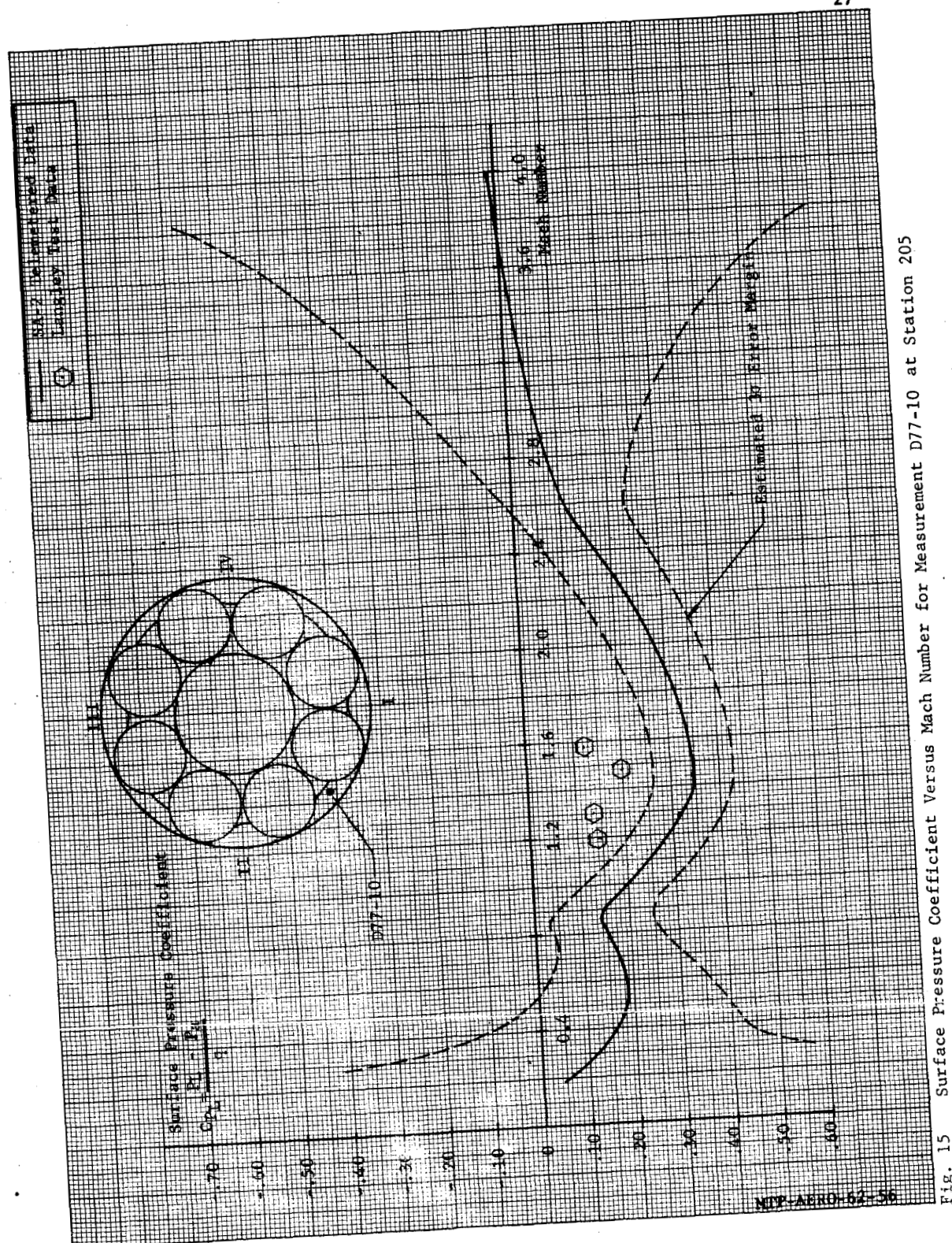
Fig. 15   Surface Pressure Coefficient Versus Mach Number for Measurement D77-10 at Station 205
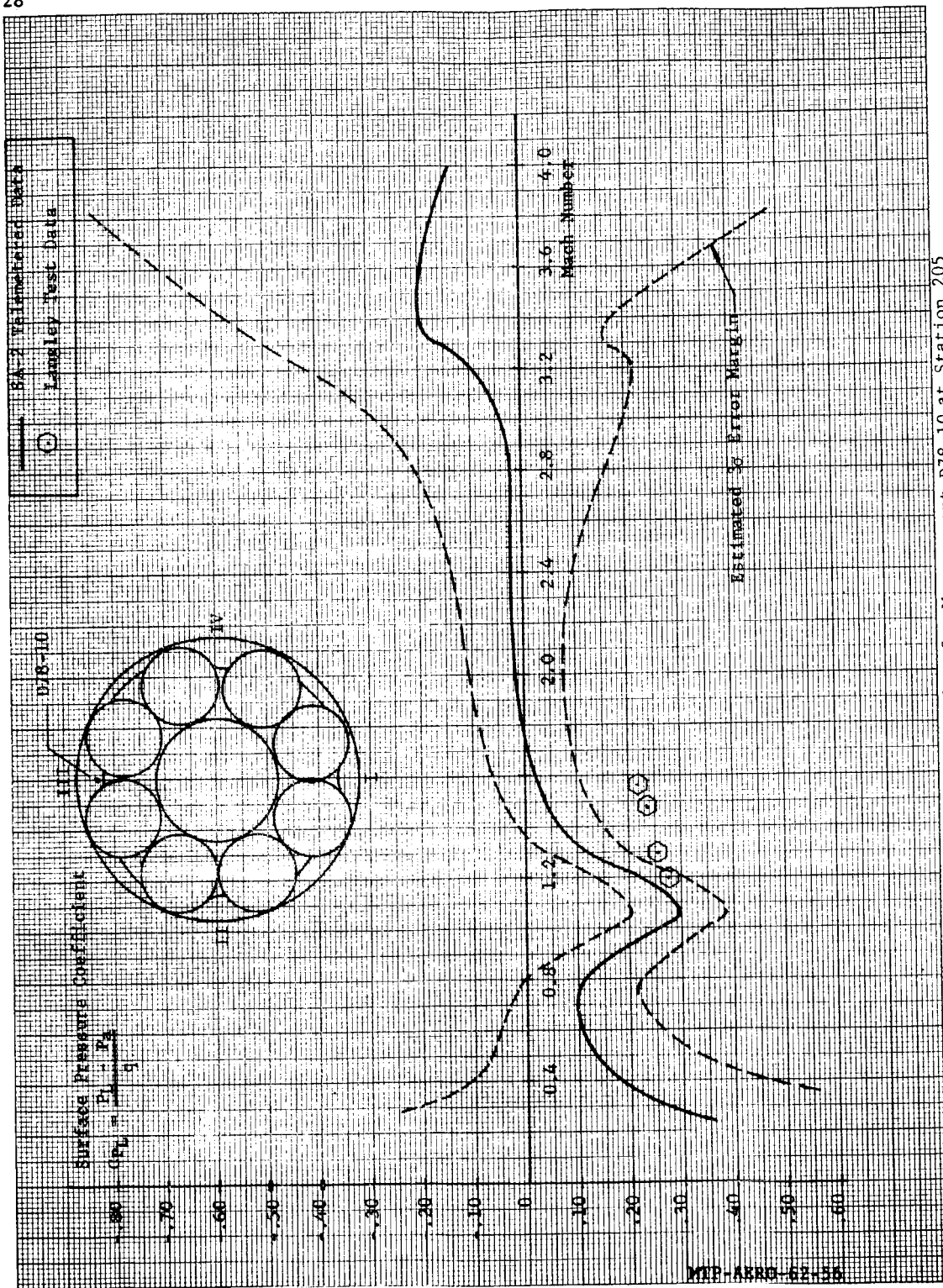
Fig. 16   Surface Pressure Coefficient Versus Mach Number for Measurement D78-10 at Station 205
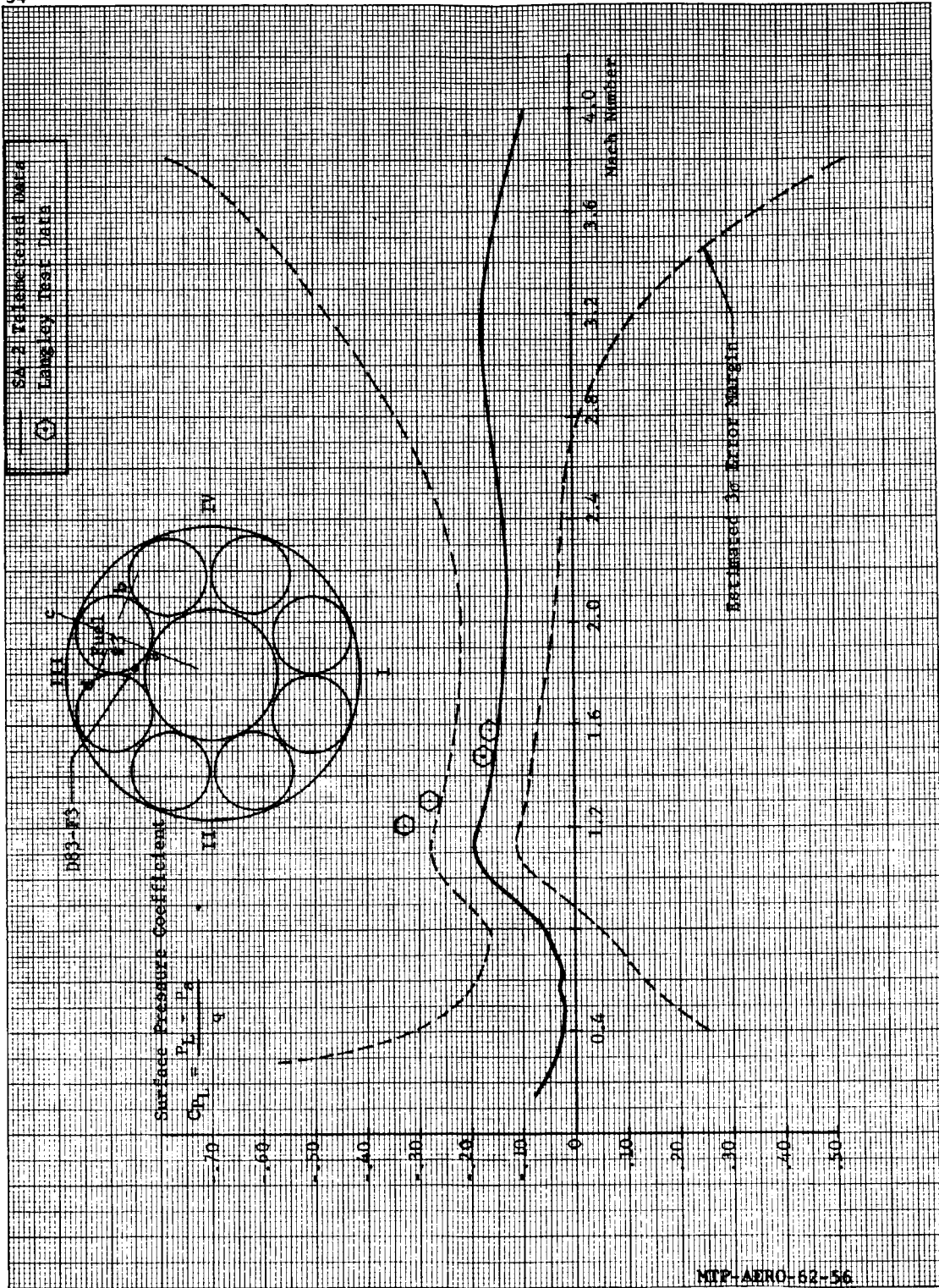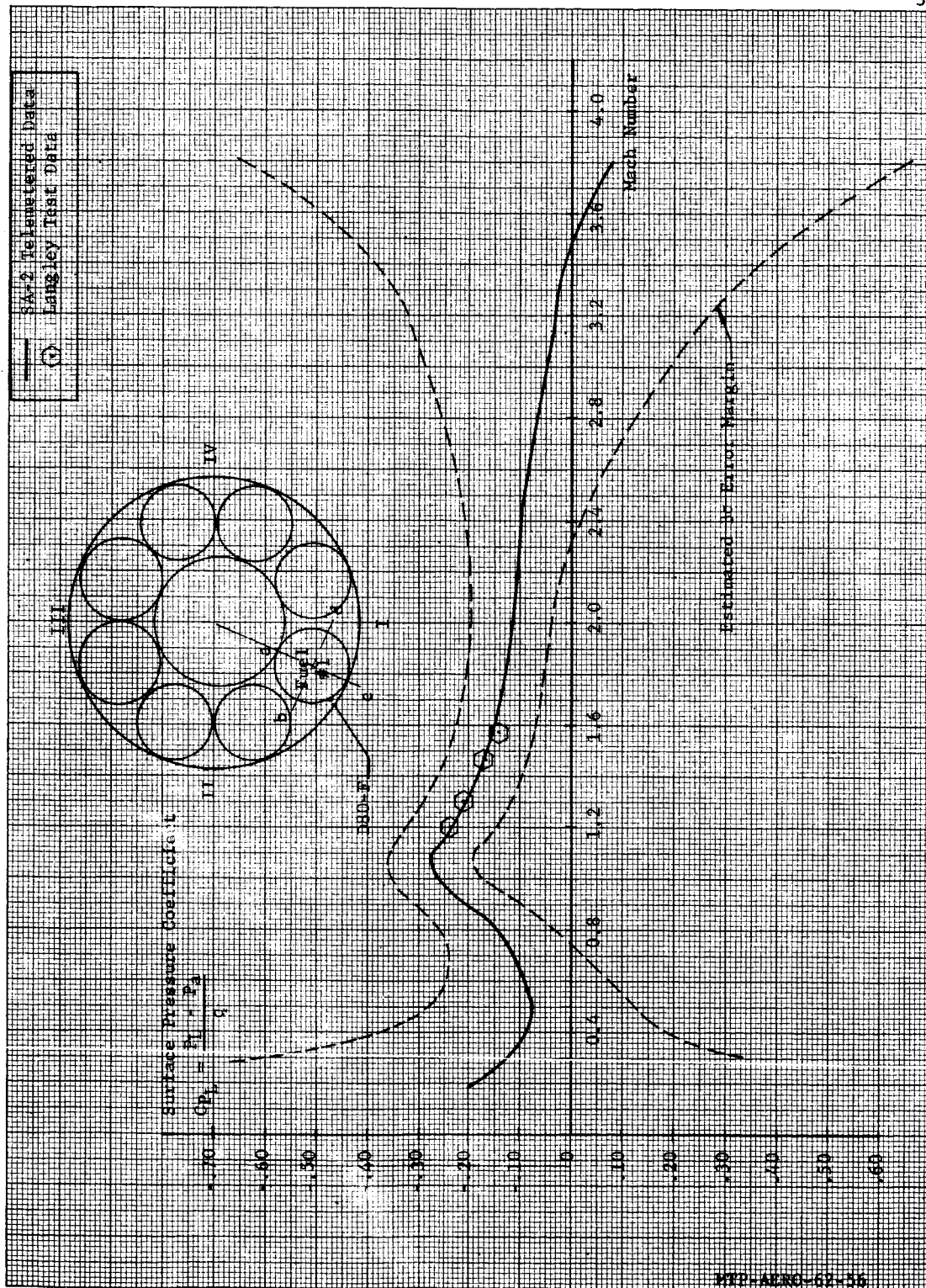
Fig. 17 Surface Pressure Coefficient Versus Mach Number for Measurement D79-10 at Station 205

7.30"

Section A-A
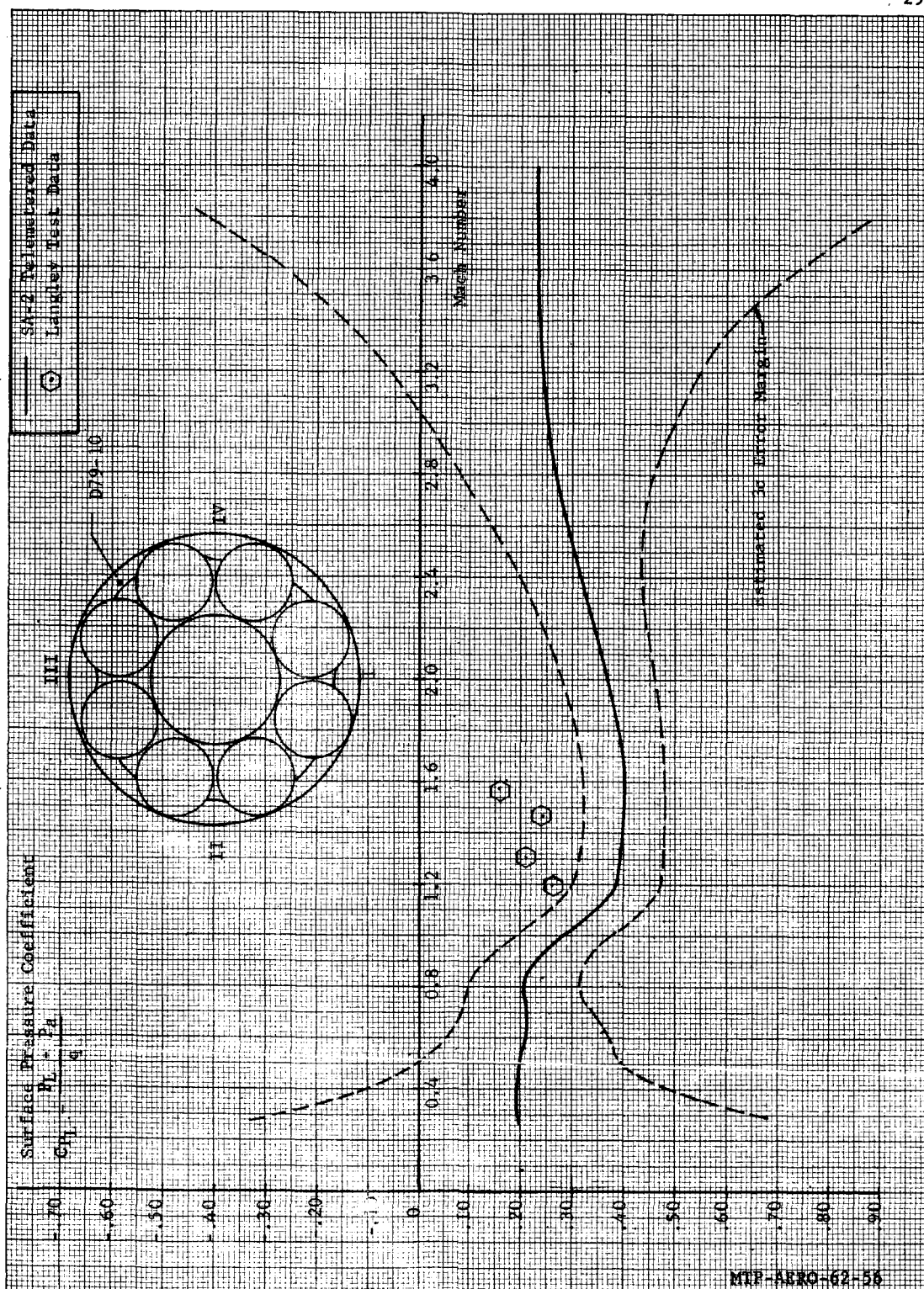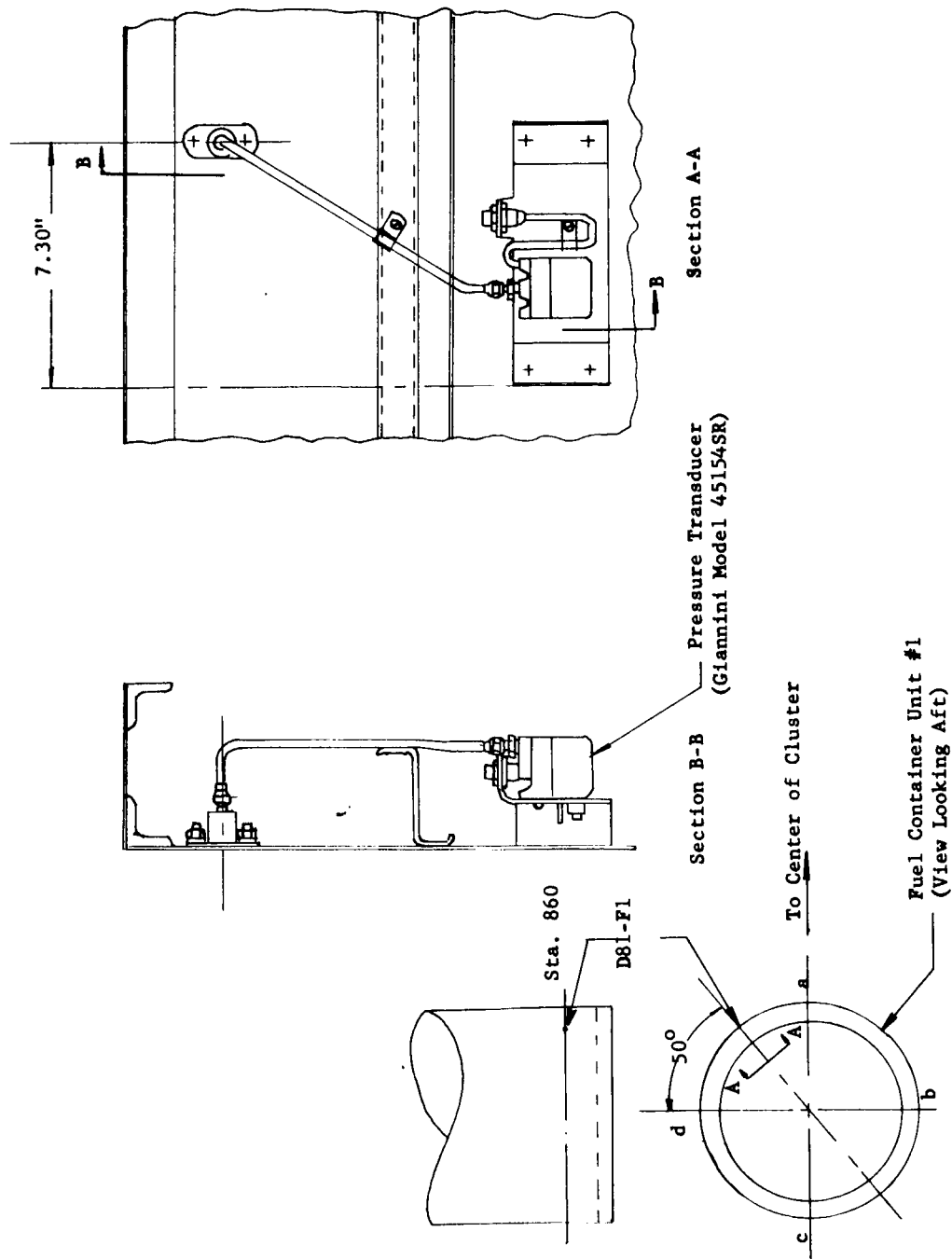
Reference E.O. No. 18-1041009

Pressure Transducer
(Giannini Model 45154SR)

Section B-B

To Center of Cluster

Fuel Container Unit #1
(View Looking Aft)

Sta. 860

D81-F1

50°

Fig. 18   Installation of Measurement D81-F1 at Station 860
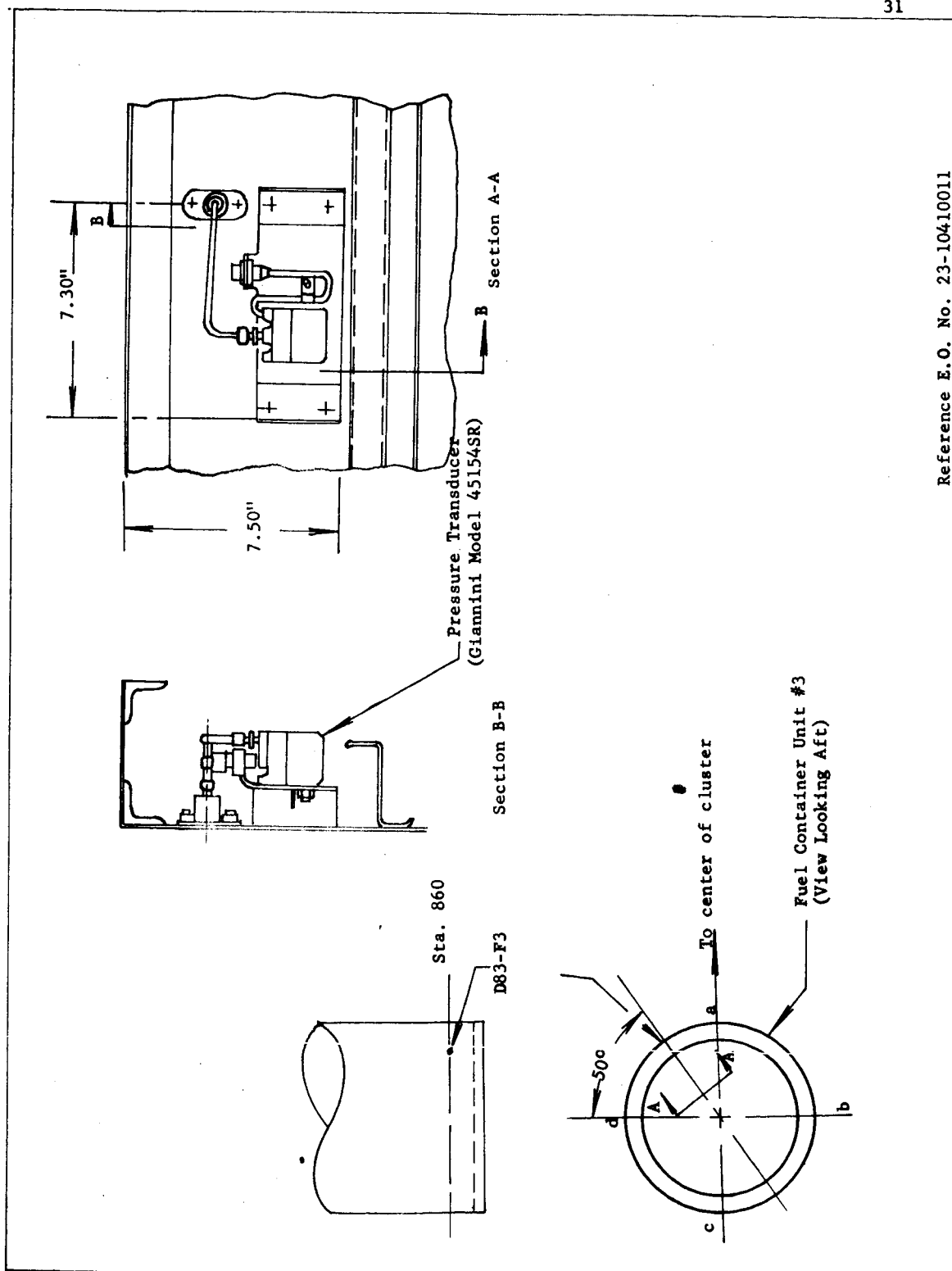
Fig. 19 Installation of Measurement D83-F3 At Station 860
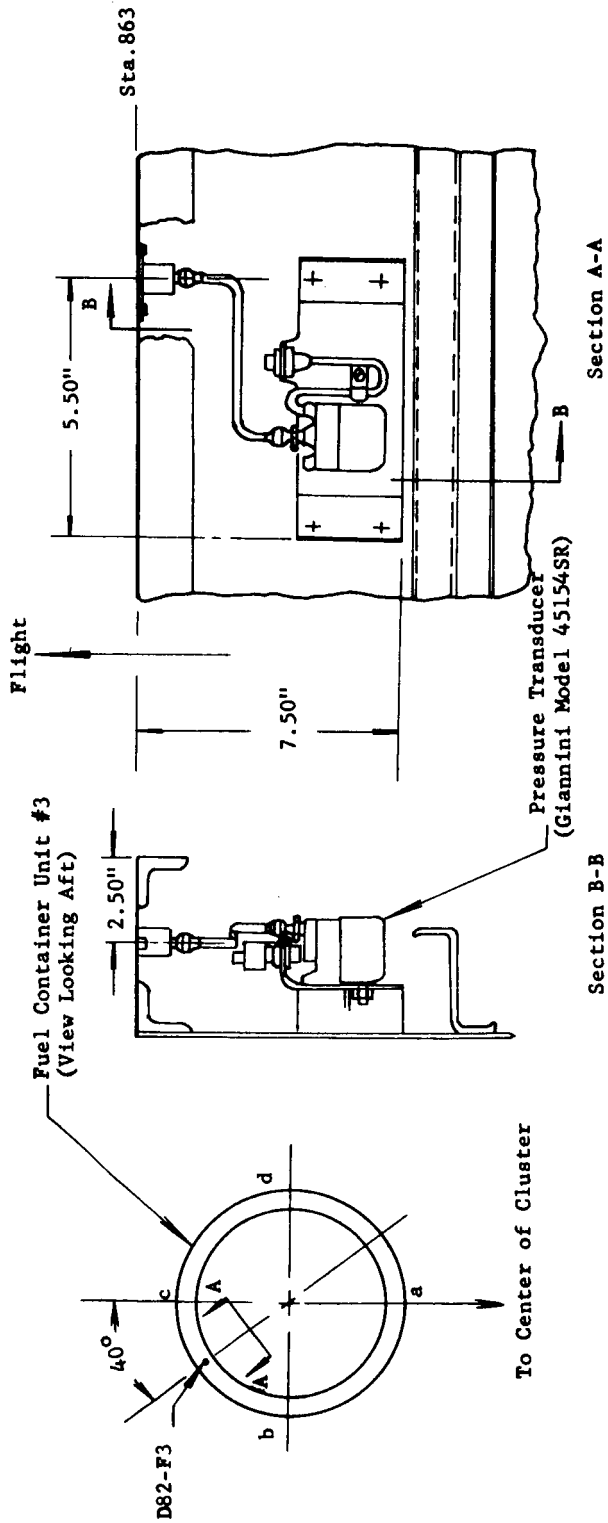
Fig. 20 Installation of Measurement D82-F3 (and D80-F1) at Station 863

MTP-AERO-62-56

Fig. 21 Surface Pressure Coefficient Versus Mach Number for Measurement D81-F1 at Station 860

34
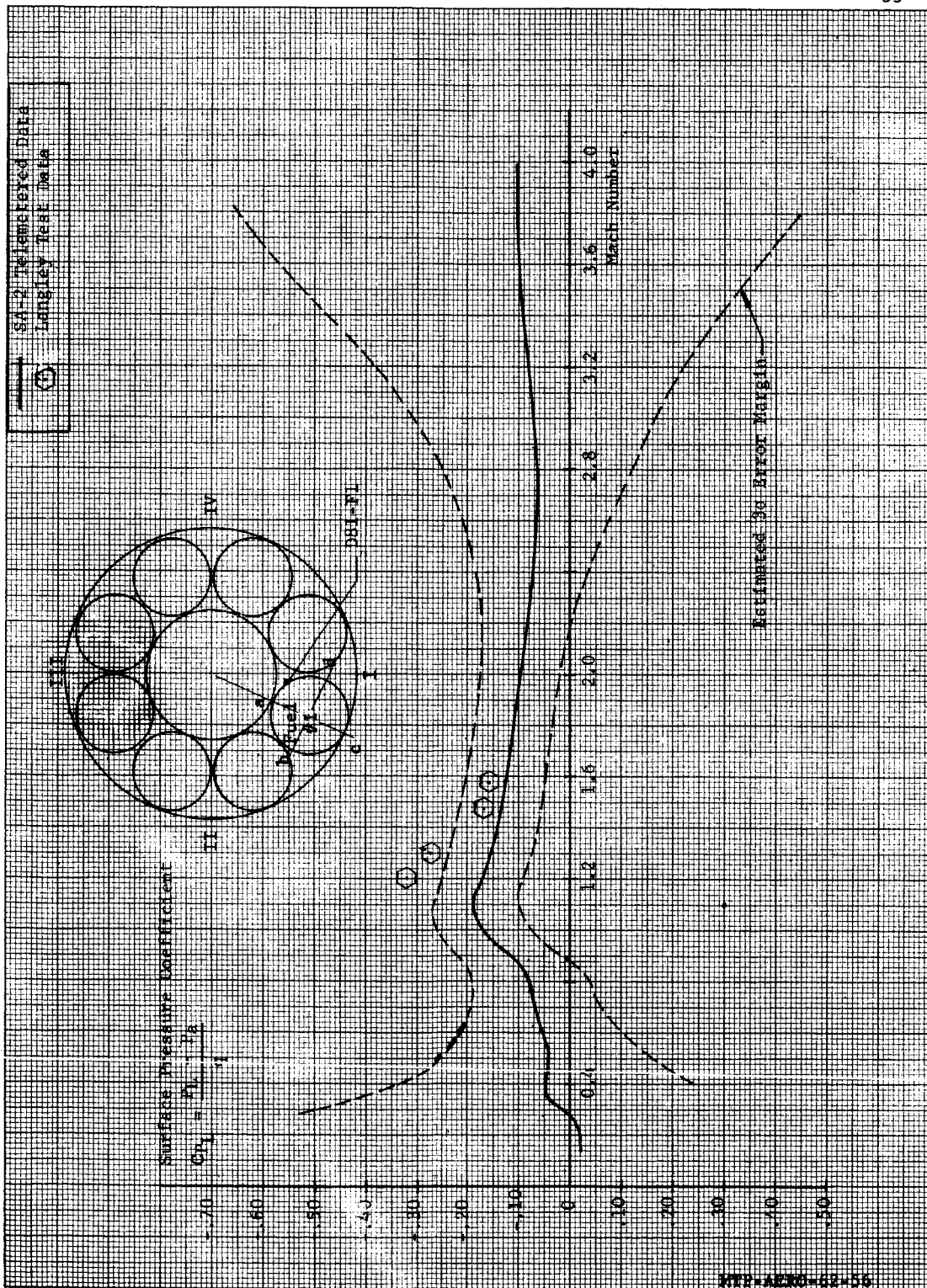
Fig. 22 Surface Pressure Coefficient Versus Mach Number for Measurement D83-F3 at Station 860

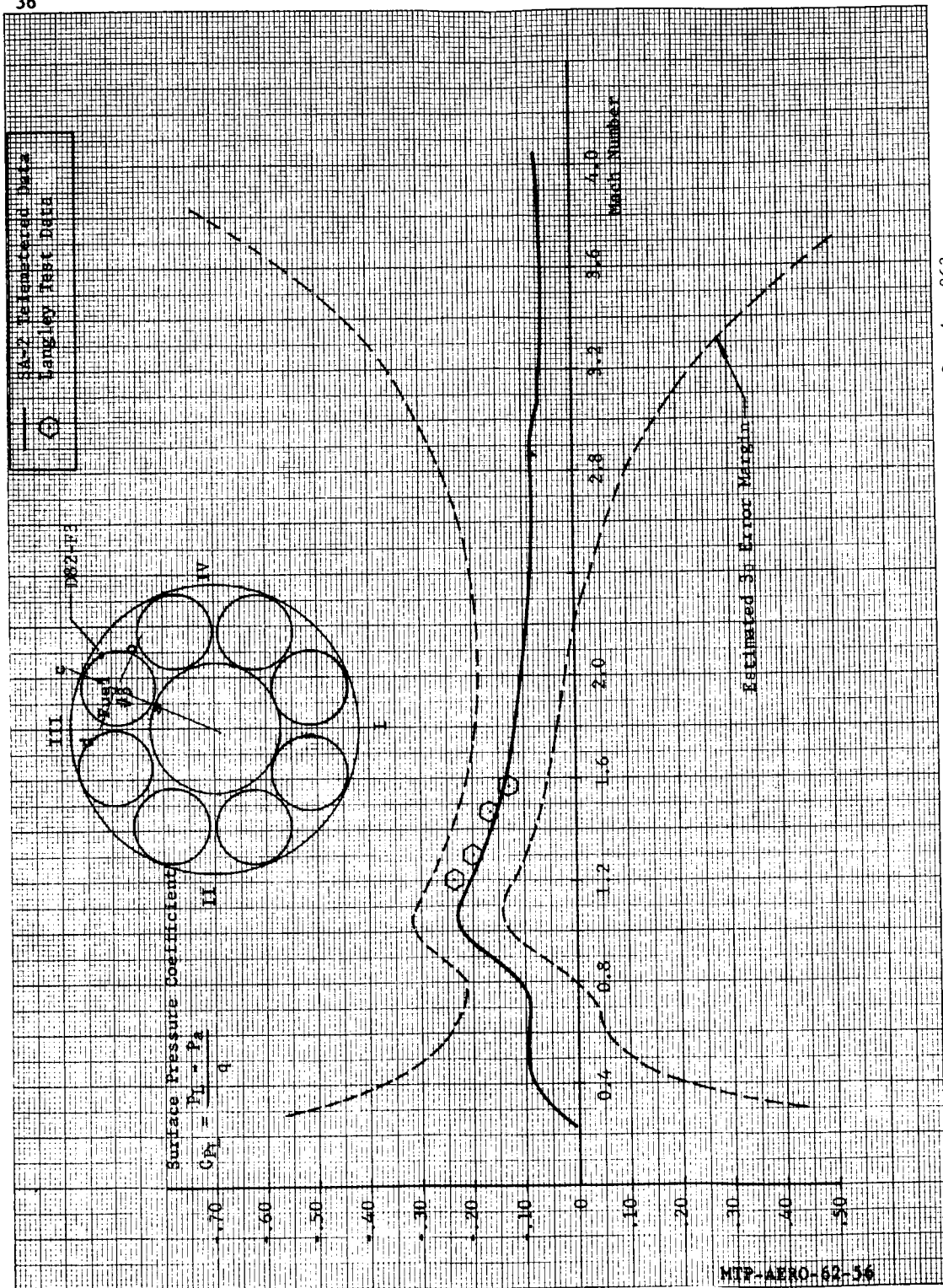Fig. 23 Surface Pressure Coefficient Versus Mach Number for Measurement D80-F1 at Station 863

36

Fig. 24   Surface Pressure Coefficient Versus Mach Number for Measurement D82-F3 at Station 863

Fig. 25 Sketch Showing Forces Acting On Vehicle Plus Stability Equations

$$C_x = \frac{F - maL}{qS}$$

$$C_z' = \frac{m\ddot{y} - \Sigma F'_o \beta}{qS\alpha}$$

$$\Sigma F'_o \beta = F'_1 \beta_1 + F'_2 \beta_2 + F'_3 \beta_3 + F'_4 \beta_4$$

$$\frac{CP}{D} = \frac{CG}{D} + \frac{1}{C_z'} \frac{1}{\alpha qSD} \left[\Sigma F'_o \beta (CG) + I\ddot{\phi} + \vartheta_t \dot{\phi} \right]$$

$$C_{m\alpha} = \left(\frac{CP}{D} - \frac{CG}{D} \right) C_z'$$
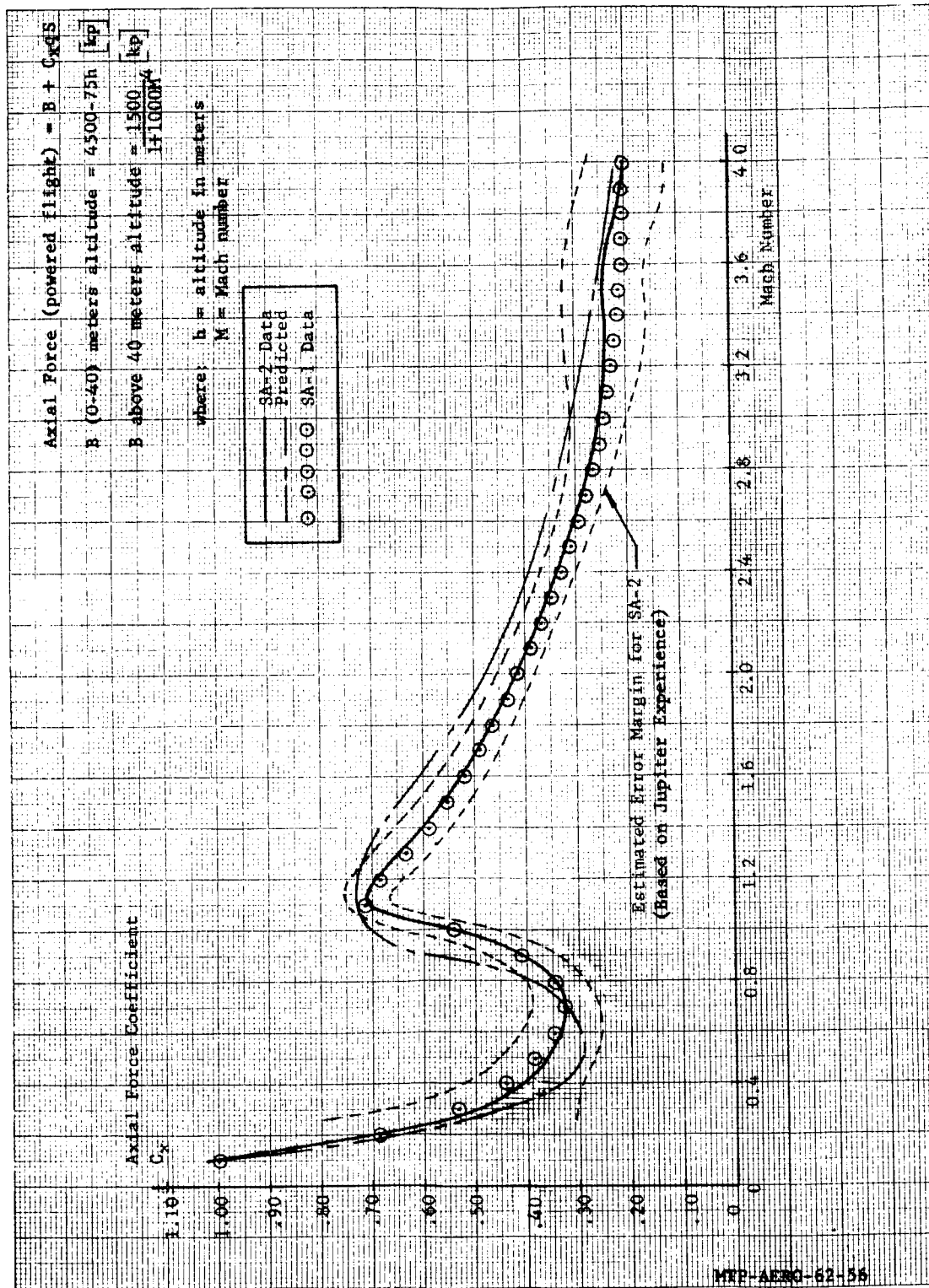
Fig. 26 Axial Force Coefficient Versus Mach Number (Power-On)
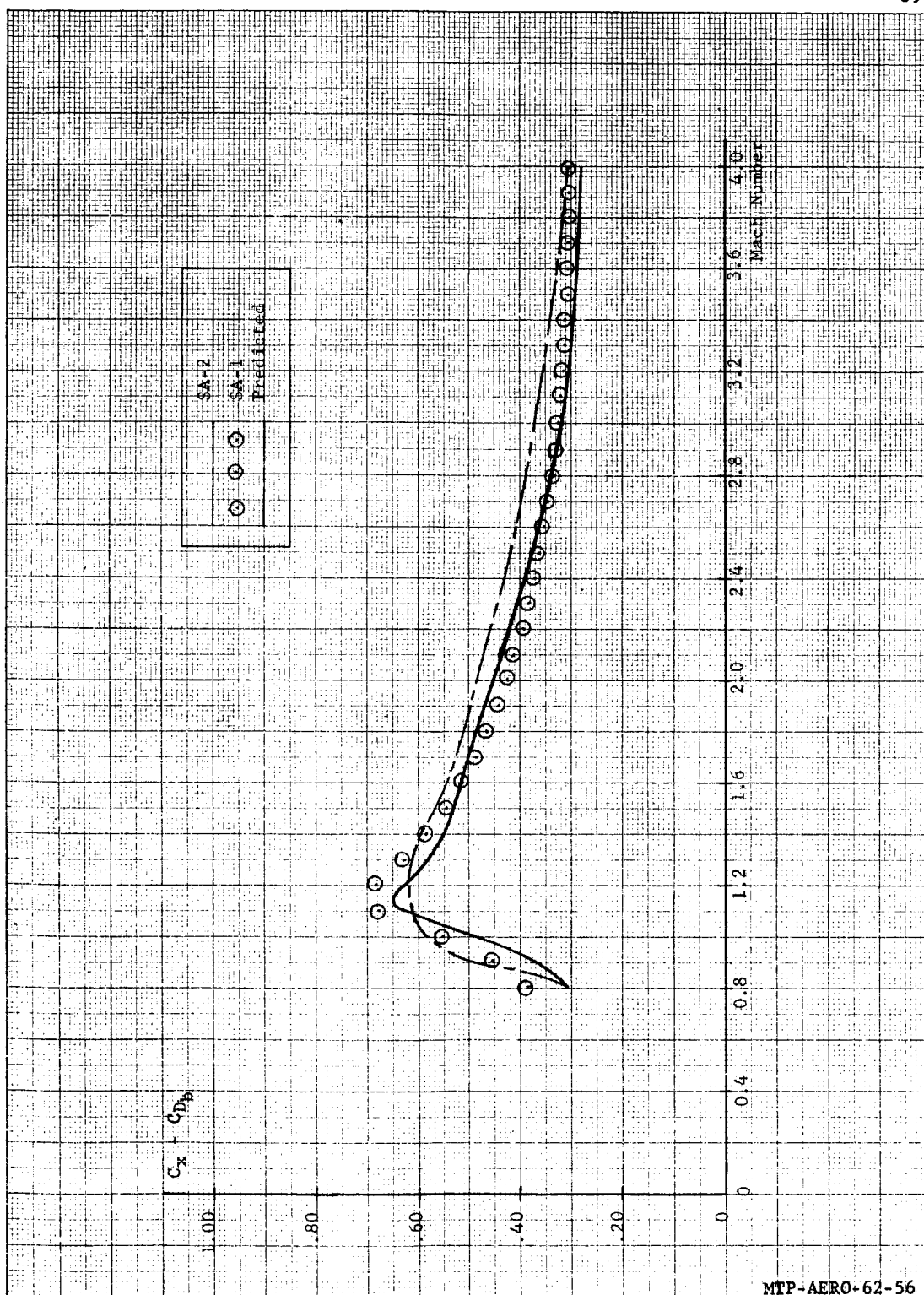
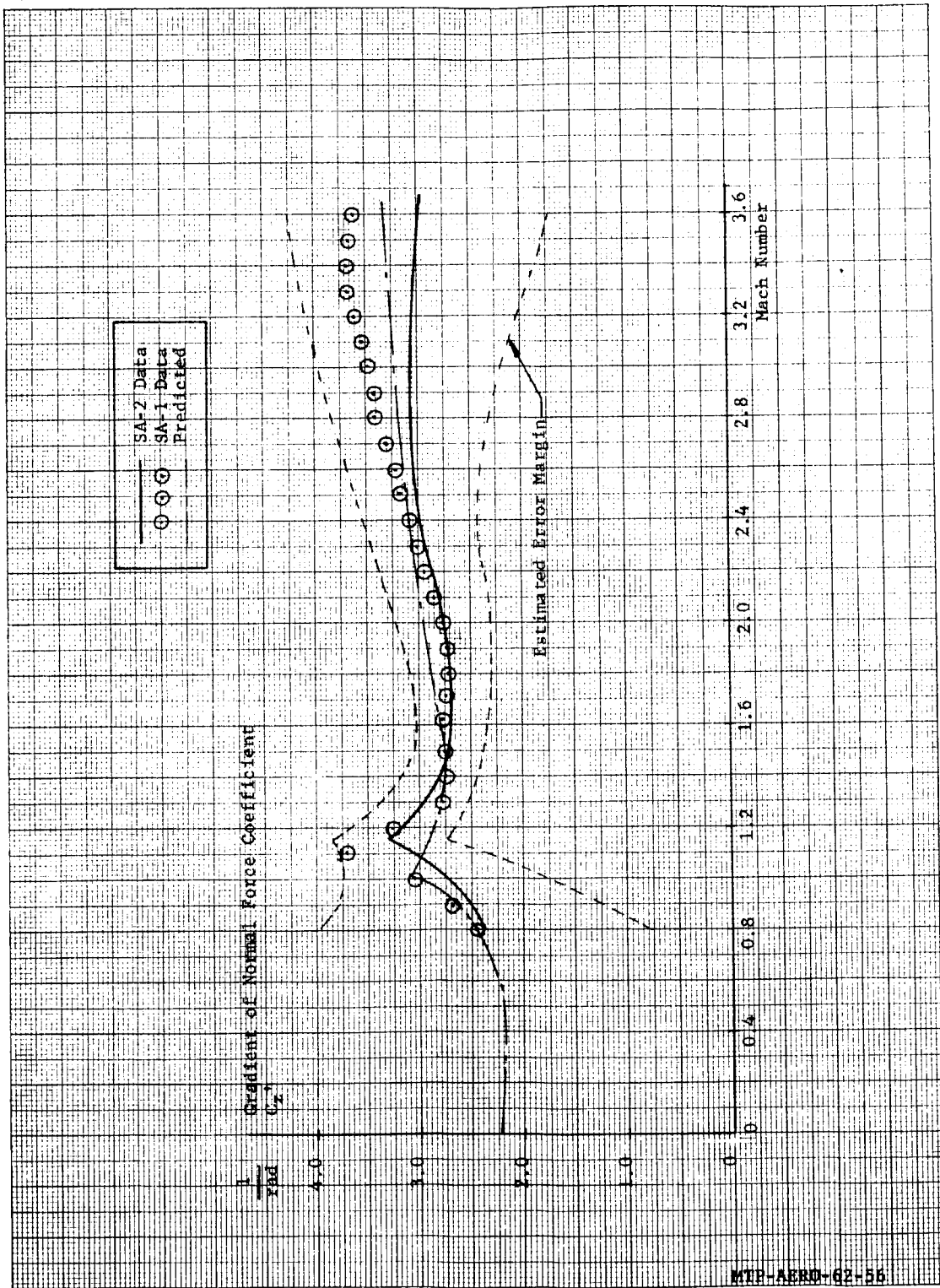Fig. 27 Axial Force Coefficient Minus Base Drag Coefficient Versus Mach Number (Power-On)

MTP-AERO-62-56

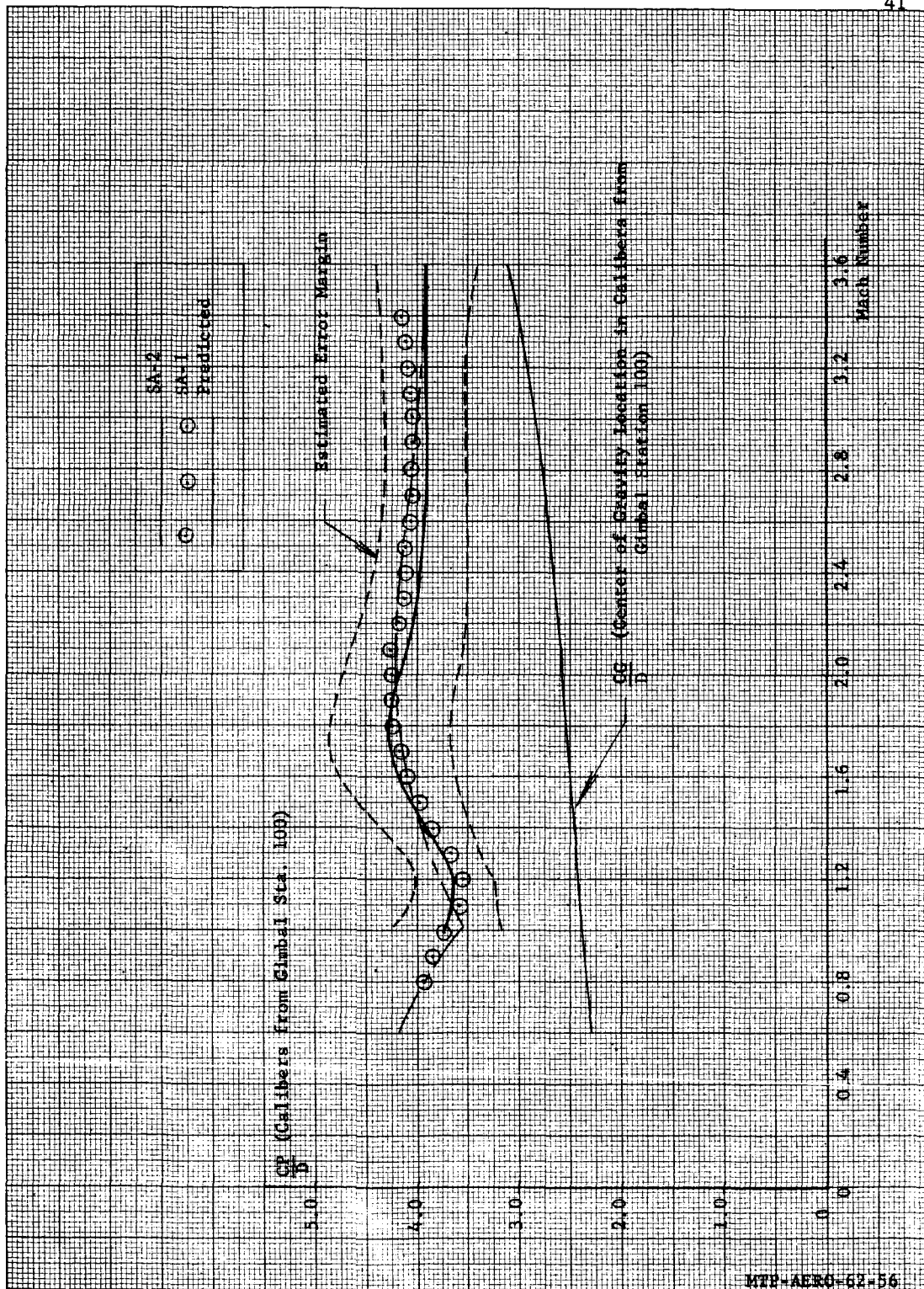Fig. 28   Gradient of Normal Force Coefficient Versus Mach Number

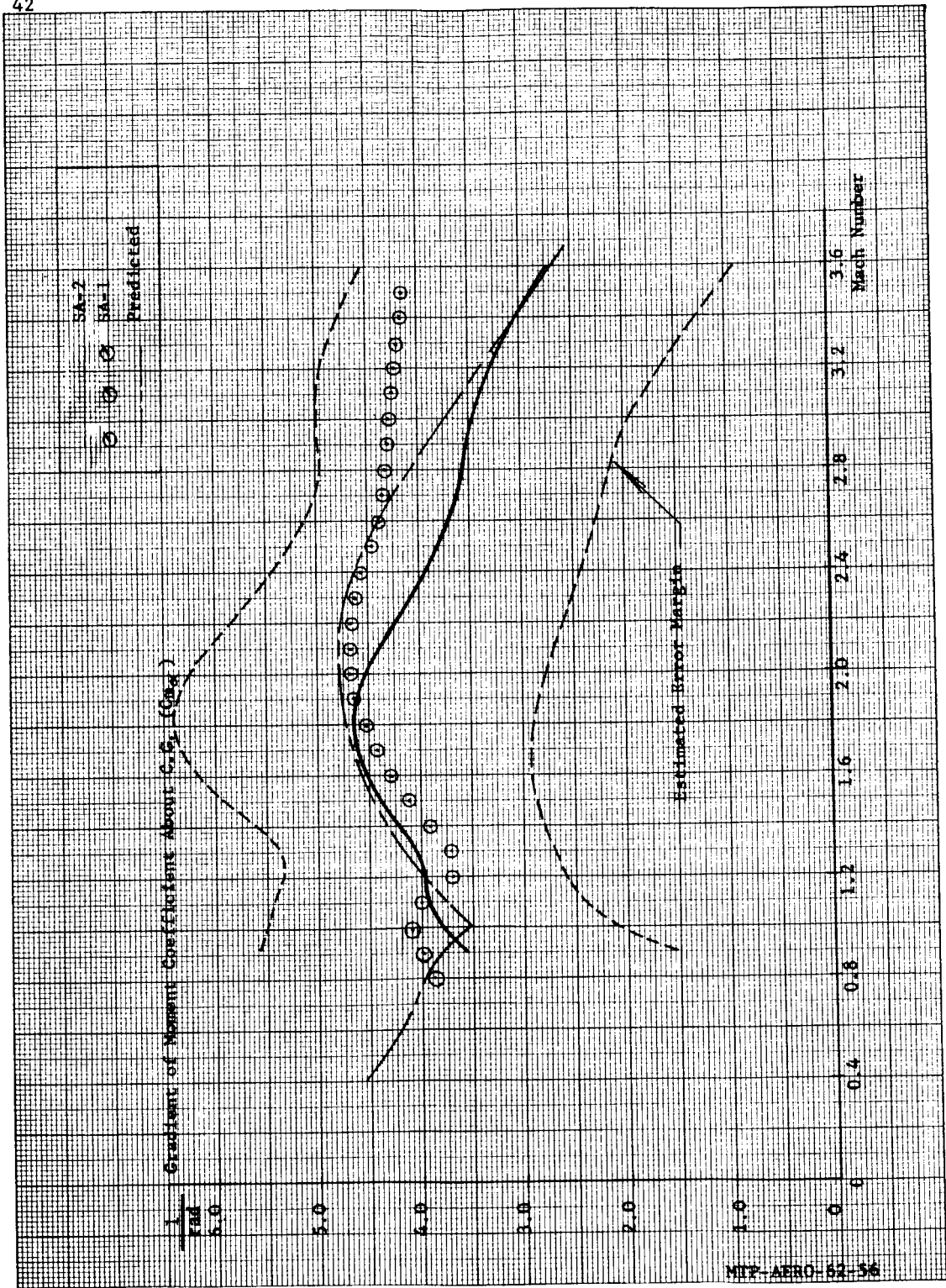Fig. 29 Center of Pressure Location Versus Mach Number

MTP-AERO-62-56

Fig. 30   Gradient of Moment Coefficient About Center of Gravity Versus Mach Number
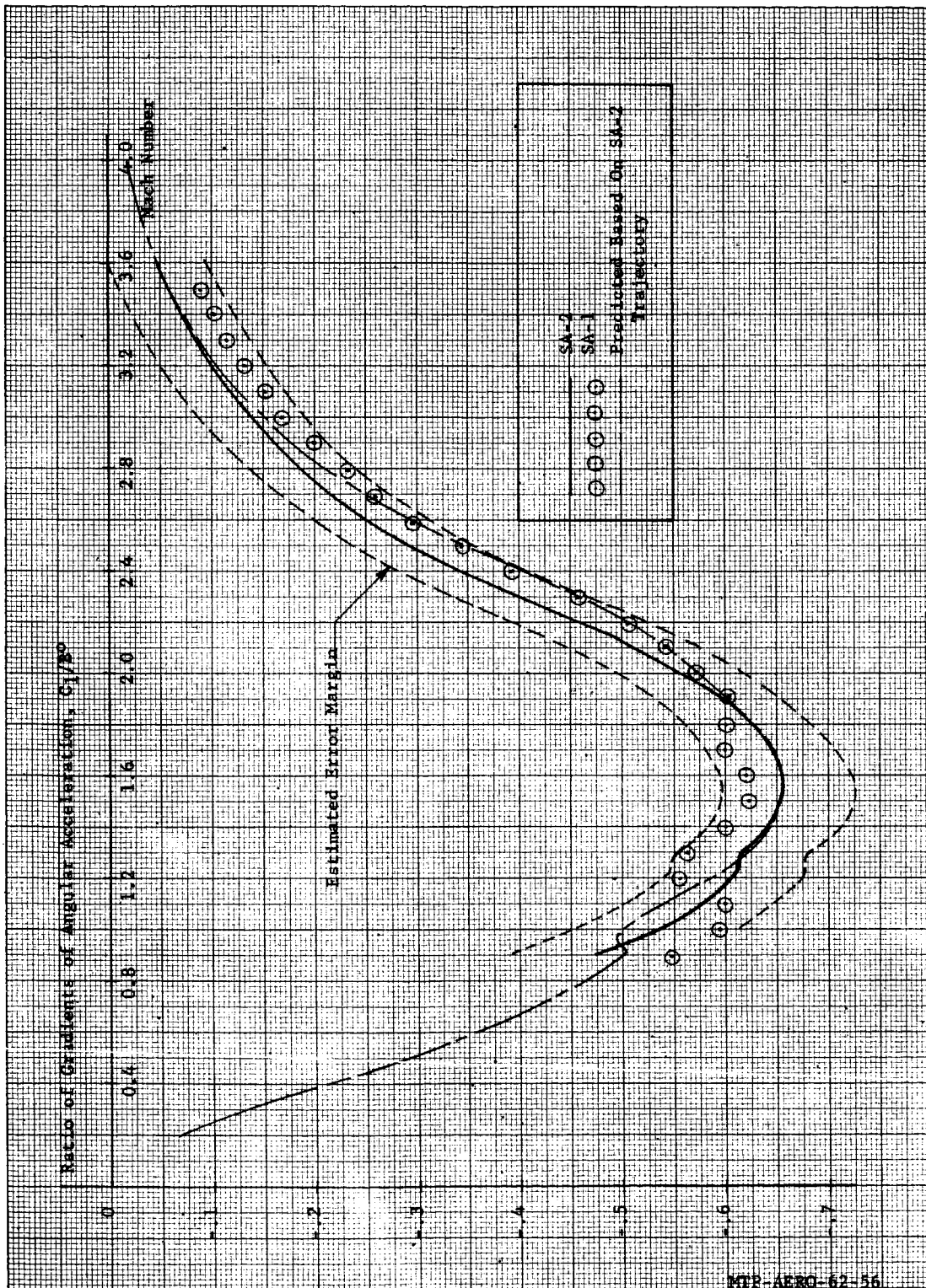
Fig. 31 Ratio of Gradients of Angular Acceleration (Stability Ratio) Versus Mach Number
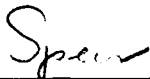
APPROVAL   MTP-AERO-62-56

AERODYNAMIC EVALUATION OF SA-2 FLIGHT (U)

By F. S. Garcia

The information in this report has been reviewed for security classifi-
cation. Review of any information concerning Department of Defense or
Atomic Energy Commission programs has been made by the MSFC Security
Classification Officer. This report, in its entirety, has been
determined to be Confidential.

_____
JAMES P. LINDBERG
Chief, Dynamics and Control Section

_____
FRIDTJOF SPEER
Chief, Flight Evaluation Branch

_____
E. D. GEISSLER
Director, Aeroballistics Division

DISTRIBUTION   MTP-AERO-62-56

M-DEP-R&D

M-AERO
    Dr. Geissler
    Dr. Speer
    Mr. Lindberg
    Mr. Garcia
    Mr. Hagood
    Mr. Payne
    Mr. Fulmer
    Mr. Dahm
    Mr. Wilson
    Mr. Linsley
    Mr. Holderer
    Mr. Weaver
    Mr. Vaughan
    Mr. Horn
    Dr. Hoelker
    Mr. O. C. Jean

M-P&VE
    Mr. Paul
    Mr. Heusinger
    Mr. Askew
    Mr. Head
    Mr. Connell

M-MS-IPL (8)

M-MS-IP

M-PAT

M-MS-H

M-HME-P